Originally published as:

"Methanol Steam Reforming"

Malte Behrens and Marc Armbrüster

Chapter 5, 2012, 175-235
DOI: 10.1007/978-1-4614-0344-9_5

In: Catalysis for Alternative Energy Generation.
Edited by Guczi, László; Erdôhelyi, András
2012, XIII, 536 p. 185 illus., 48 in color., Hardcover

ISBN: 978-1-4614-0343-2

Methanol Steam Reforming

Malte Behrens[a,*] and Marc Armbrüster[b]

a. Department of Inorganic Chemistry, Fritz-Haber-Institute, Faradayweg 4-6, 14196 Berlin, Germany

b. Max-Planck-Institut für Chemische Physik fester Stoffe, Nöthnitzer Strasse 40, 01187 Dresden, Germany

* email: behrens@fhi-berlin.mpg.de, Tel: +49 30 8413 4408

Outline

Catalysis: Alternative Energy Generation – Methanol Steam Reforming 1

Introduction 2

Cu-based Catalysts for Methanol Steam reforming 8
General aspects of Cu/ZnO-based catalysts 10
Drawbacks of Cu/ZnO-based catalysts 14
Preparation of Cu/ZnO-based catalysts 21
Ternary Cu/ZnO/X catalysts (X = Al_2O_3, ZrO_2) 32
ZnO-free Cu-based catalysts 38
The active form of Cu under MSR conditions 43

Intermetallic Compounds in Methanol Steam Reforming 51
Catalysts derived by decomposition of intermetallic compounds 57
Supported intermetallic compounds 61
Unsupported intermetallic compounds 76

Introduction

The currently increasing interest in catalytic reactions of methanol, CH_3OH, is – in addition to its customary role as an important base chemical and feedstock for value-added molecules – due to its potential as a chemical storage molecule for hydrogen. Methanol is industrially produced from natural gas- or coal-derived syngas, but can in principle also be synthesized from CO_2 by hydrogenation [1]. It is suggested by Olah et al. [2] as a "CO_2-neutral" combustion fuel in the context of the so-called methanol economy or can be used in direct methanol fuel cells (DMFC) for generation of electric power. Methanol might thus play a key role in the transition towards a future energy scenario, which has to be more and more independent from fossil sources [3].

The main advantage of using methanol for chemical instead of physical storage of hydrogen is related to its decentralized use of hydrogen, e.g. in the transportation sector. Methanol is a very attractive onboard hydrogen source for polymer electrolyte fuel cells (PEMFC) in mobile applications like automobiles as it circumvents the problems of physical storage and distribution of hydrogen such as the necessity of pressurized or cryogenic containers. Methanol is liquid at ambient conditions and can be safely distributed using pipelines and conventional filling station infrastructure. It has a high H:C ratio of 4:1 and no C-C bond, which has to be broken.

There are several catalytic reactions available for liberating hydrogen from methanol:

Methanol decomposition (MD):

$$CH_3OH \rightarrow CO + 2\ H_2 \qquad \Delta H^0 = 90\ kJ/mol\ (1)$$

Methanol steam reforming (MSR):

$$CH_3OH + H_2O \rightarrow CO_2 + 3\ H_2 \qquad \Delta H^0 = 49\ kJ/mol\ (2)$$

Partial oxidation of methanol (POM):

$$CH_3OH + 0.5\ O_2 \rightarrow CO_2 + 2\ H_2 \qquad \Delta H^0 = -155\ kJ/mol\ (3)$$

Furthermore, the water gas shift (WGS) and reverse WGS (rWGS) reactions have to be considered:

$$CO + H_2O \rightarrow CO_2 + H_2 \qquad \Delta H^0 = -41\ kJ/mol\ (4)$$

Among these reactions, MSR seems to be most attractive as it generates the highest hydrogen concentration in the product stream, runs at relatively low temperatures of 500 – 600 K, and does not directly produce CO, which acts as a poison for the downstream PEMFC anode catalyst. MSR was first described in 1921 by J. A. Christiansen [4] and research on its application for hydrogen production has a long history [5]. The recently renewed interest was triggered by the development of fuel cell technology requiring clean and preferably renewable hydrogen. A number of general overview articles and reviews are available addressing the role of MSR in this context [e.g.

5-11]. MSR is an endothermic reaction and requires external heating. It is sometimes used in combination with exothermic POM (autothermal reforming or oxidative steam reforming) [12,13] or combustion of methanol [8] in order to generate the necessary heat. However, the endothermicity of MSR is much weaker compared to steam reforming of other hydrocarbons or higher alcohols [8] and reformer units can be relatively small enabling the onboard combination with PEMFCs. Several prototype vehicles that run on hydrogen fuel cell technology have already been developed by different companies. A comparison between methanol and other molecules as reactants for onboard hydrogen production can be found in the comprehensive review by Palo et al. and in the references therein [11].

This chapter will focus mainly on the challenges of catalyst development for MSR. The requirements for a good MSR catalyst to be used for onboard hydrogen production in combination with PEMFCs are the following:

- The catalyst should be highly selective to CO_2 and minimize the CO content in the hydrogen-rich product gas stream, which acts as a poison for PEMFC anodes.
- It should be active at low temperatures to be efficient and to disfavor the rWGS reaction as a source of CO.
- Its components should be abundant and of low cost and its preparation should be facile and scalable.

- It should be stable at extended time on stream, i.e. resistant to coke formation, stable against sintering and tolerant towards catalyst poisons.
- In particular, it should be stable towards abrupt changes of the conditions of reforming, i.e. work reliably in transient situations like on-off operations as well as in steady state to produce sufficient amounts of hydrogen on demand.

The detrimental role of CO in the effluent for the downstream PEMFC is to be emphasized. CO chemisorbs irreversibly on the typically Pt-based fuel cell catalysts and causes irreversible site blocking. Its concentration has to be below ca. 20 ppm in order to prevent poisoning, which is usually not achieved in the reformer outlet gas. Thus, in technical applications, a gas purification step has to be introduced between reformer and fuel cell. The CO concentration in the gas stream can lowered by means of preferential oxidation (PROX) or using Pd membranes, which in both cases complicates the setup and generates costs [14]. Generally, a low selectivity to CO – in addition to high activity and stability – is, thus, a major and particular requirement for a successful MSR catalyst.

This chapter is divided into two parts treating different families of catalytic materials active in the MSR reaction. The first part covers the widely studied Cu-based catalysts, while the second part will focus on the role of intermetallic compounds in MSR. Some catalytic

data from the literature for the MSR reaction over selected catalysts treated in this chapter is compiled in Table 1.

Tab. 1: Comparison of catalytic performance in (oxidative) MSR of selected catalyst systems covered in this contribution. Note possible difference in feed gas composition and contact time of the experiments. Some values were re-calculated from the data given in the original references.

Catalyst	**Pre-treatment[a]**	**Conversion / %**	**CO_x formation / %**	**H_2 production rate / $Lg^{-1}h^{-1}$**	**T / K**	**Remarks[b]**	**Ref.**
43.8% Cu/ZnO	C623 R523	90	0.14[c]	-	582	(Co-ppt.)	[15]
39.4% Cu/ZnO/Al_2O_3	C623 R573	90	0.11[c]	-	579	(Co-ppt.)	[15]
32.3% Cu/ZnO/ZrO_2	C623 R573	90	0.05[c]	-	567	(Co-ppt.)	[15]
30.9% Cu/ZnO/Al_2O_3/ZrO_2	C623 R573	90	0.05[c]	-	551	(Co-ppt.)	[15]
Cu/ZnO/Al_2O_3	C723 R723	90	<0.05[c]	38.4	673	18 mol% Cu in LDH (Co-ppt.), oMSR	[16]
61.7% Cu/ZnO/Al_2O_3	R523	84.4	0.11[c]	1.4	523	(commercial)	[17]
32.3% Cu/ZnO/ZrO_2	C723 R573	71.7	0.22[c]	8.7	503	(Co-ppt.), oMSR	[18]
35.5% Cu/ZnO/CeO_2	C723 R523	66.8	0.23[c]	8.2	503	(Co-ppt.), oMSR	[18]
8.5% Cu/ZrO_2	C773 R523	92	0.2[c]	-	523	(Templ. method)	[19]
16% Cu/ZrO_2	C673 R523	57	0.02[c]	-	523	(ME method)	[20]
3.9% Cu/CeO_2	C723 R673	90.7	2.3[d]	10.9	533	(Co-ppt.)	[21]
3.9% Cu/ZnO	C723 R673	66.8	0.9[d]	8.0	533	(Co-ppt).	[21]
3.9% Cu/Al_2O_3	C723 R673	21.5	0.4[d]	2.6	533	(Co-ppt.)	[21]
QC-$Al_{63}Cu_{25}Fe_{12}$[f]	R523	-	-	14.1	573	L:NaOH	[22]
$CuAl_2$		-	-	3.81	513	L:NaOH/	[23]

						Na_2CrO_4	
Ni_3Al	R523	10	6[e]	56[g]	793		[24]
A-$(Cu_{50}Zr_{50})_{90}Au_{10}$[f]	C550	80	100[e]	14.0	523		[25]
10% Pd/SiO_2	R573 C773	15.7	0[e]	2.82	493		[26]
10% Pd/Al_2O_3	R773 C773	67.4	0[e]	12.14	493		[26]
10% Pd/ZnO	R773 C773	55	99.8[e]	9.80	493		[26]
10% Pt/SiO_2	R773 C773	25.6	0.3[e]	4.61[h]	493[h]		[27]
10% Pt/ZnO	R773 C773	27.6	95.4[e]	4.96	493		[26]
2% Pt-Zn/C	R773 R873	100	83[e]	1.12	553	Zn/Pt = 5.0	[27]
2% Pt/C	R873	76	48[e]	0.84	553		[27]
10% Pt/In_2O_3	C773	30.6	98.3[e]	5.51	493		[28]
10% Pt/Ga_2O_3	R773 C773	5.4	75.5[e]	0.97	493		[28]
10% Pd/Ga_2O_3	R773 C773	21.2	94.6[e]	3.82	493		[26]
10% Pd/In_2O_3	R773 C773	28.3	95.5[e]	5.10	493		[26]
15% Pd-In/Al_2O_3	R773 C673	91	98.7[e]	68.25	698	In/Pd = 2	[29]
8.9% Pd-Zn/Al_2O_3	C623	46.5	99.4[e]	4.1	493	Zn/Pd = 2.6	[30]
8.6% Pd/ZnO	R673 C623	14.3	99.2[e]	1.6	493		[30]
10% Ni/ZnO	R673 C773	15.7	4.7[e]	2.83[h]	493[h]		[27]
10% Ni/SiO_2	R773 C773	7.3	1.1[e]	1.31[c]	493[c]		[27]
10% Co/ZnO	R773 C773	20.3	8.9[e]	3.65[h]	493[h]		[27]
Pd black	R773 R513	7[i]	2[e]	13.3	533		[31]
ZnPd	R513	7[i]	100[e]	2.6	533		[31]
PtZn	R513	7[i]	50[e]	2.6	533		[31]
PdCd	R513	7[i]	100[e]	2.6	533		[31]
NiZn	R513	7[i]	15[e]	2.6	533		[31]

[a] calcination (C) and reduction (R) temperatures in K

[b] Methods of preparation (Co-ppt. = co-precipitation, templ. method = template method, ME method = microemulsion method, LDH = layered double hydroxide, L = leaching agent), oMSR = oxidative MSR
[c] given as CO concentration in the product gas
[d] given as selectivity towards CO
[e] given as selectivity towards CO_2
[f] QC:quasicrystalline, A: amorphous
[g] in $Lh^{-1}m^{-2}$
[h] derived from comparison to data from [26]
[i] 7% to 10% given

Cu-based Catalysts for Methanol Steam reforming

Cu-based catalysts are widely used in C1 chemistry. This is mostly due to the commercial interest in the most common industrial methanol synthesis catalyst, a complex $Cu/ZnO/Al_2O_3$ bulk catalyst, which is also active in MSR and fulfills many of the requirements mentioned above, such as high activity at low temperature, relatively low CO levels, and feasible and scalable – though complex – preparation at moderate costs. Commercial ternary $Cu/ZnO/Al_2O_3$ catalysts or the unpromoted binary Cu/ZnO model system were thus employed in many studies of MSR and this material will be discussed in detail below. While preparation and composition of the industrial catalyst $Cu/ZnO/Al_2O_3$ can be regarded as already highly optimized for application under methanol synthesis conditions, modifications of the Cu/ZnO/X system turned out to improve the properties of Cu-based catalysts for use in MSR. In particular, choosing another second oxide phase X or employing new catalyst precursors like layered double hydroxides, or even changing to ZnO-free samples and using zirconia or ceria for preparation of Cu-based catalysts

was reported to lead to interesting MSR performance. The state of the active Cu surface under reaction conditions and the nature of the active sites are still debated in literature and will be discussed in this section.

Several studies are available addressing the mechanism and kinetics of the MSR reaction over Cu based catalysts [32-38]. There seems to be agreement nowadays that CO_2 is a direct product of the MSR reaction and not of a sequence of MD and WGS reactions. The main source of CO is the rWGS reaction taking place as a secondary reaction after MSR. Frank et al. [38] presented a comprehensive microkinetic analysis of the MSR reaction based on the work of Peppley et al. [34]. They investigated several Cu-based catalysts with various oxide components showing considerably different activities. Similar activation energies support the idea that the surface chemistry is independent of the oxide material (with the exception of $Cu/Cr_2O_3/Fe_2O_3$, which behaved differently). Dehydrogenation of methoxy groups is the rate limiting step and by means of DRIFTS experiments methoxy and formate species were found as the dominating species at the surface. Two distinct kinds of active sites were considered, S_A for the adsorption and desorption of oxygenates and S_B for hydrogen (Fig. 1) and two reaction pathways of the methoxy intermediate are discussed via dioxomethylene, the intermediate of the reverse methanol synthesis reaction, or methyl formate. On basis of the kinetic data it was not possible to decide which route was dominant.

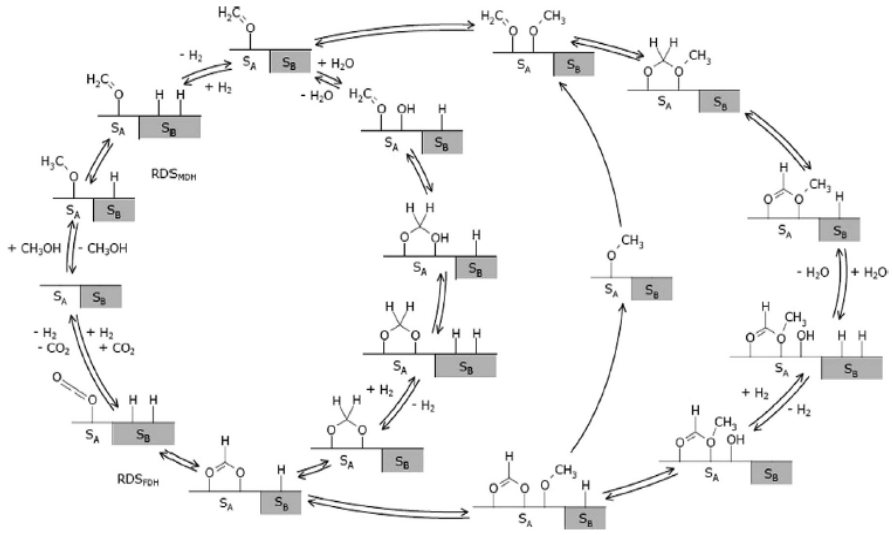

Fig. 1: Catalysis cycle for MSR over Cu-based catalysts based on the work in refs [32-34] including two different kinds of reactive sites S_A and S_B. Reprinted from ref [38] with permission from Elsevier.

General aspects of Cu/ZnO-based catalysts

Commercial $Cu/ZnO/Al_2O_3$ methanol synthesis catalysts are often mistaken as supported systems, but neither ZnO nor Al_2O_3 represent classical extended oxidic supports. This is obvious, when considering the typical composition of modern $Cu/ZnO/(Al_2O_3)$ catalysts, which is characterized by a molar Cu:Zn ratio close to 70:30, while the amount of Al_2O_3 typically is significantly lower than that of ZnO. This Cu-rich composition manifests itself in a peculiar microstructure of the industrial $Cu/ZnO/Al_2O_3$ catalyst (Fig. 2) [39], which is composed of spherical Cu nanoparticles of a size < 10 nm and often even smaller ZnO nanoparticles arranged in an alternating fashion. Thus, porous aggregates are formed (Fig. 2d) in which the oxide particles act as spacers between Cu particles (Fig. 2e). The

presence of inter-particle pores as seen in the HRTEM image allows some access to the "inner surface" of larger Cu/ZnO aggregates. This unique microstructure, represented in Figure 2b, can be described as an intermediate stage between a supported catalyst, schematically drawn in Figure 2a, and a bulk metallic sponge or skeletal Raney-type catalyst, represented in Figure 2c.

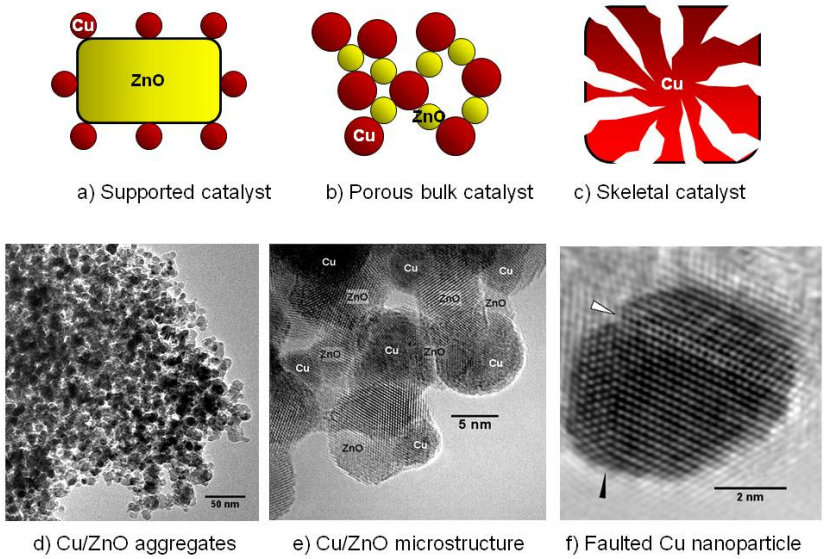

Fig. 2: Schemes of different catalyst microstructures (a-c) and transmission electron micrographs of a Cu/ZnO/(Al_2O_3) catalyst (d-e). In the high resolution image (f) planar defects of the Cu-nanoparticles like twin boundaries (black arrow) and stacking faults (white arrow) can be seen.

It is this unique microstructure, which enables a reasonably high dispersion of Cu and exposure of many Cu-ZnO interfaces at a high total Cu content. The specific Cu surface area (SA_{Cu}) of methanol catalysts can be determined by reactive N_2O titration [40], which causes surface oxidation of the Cu particles and allows estimation of

SA_{Cu} from the amount of evolved N_2, as N_2O is decomposed at the metallic Cu surface, or from the H_2 consumption upon re-reduction. Assuming formation of an oxygen monolayer, a surface stochiometry corresponding to Cu_2O and an abundance of 1.47×10^{19} oxygen atoms/m^2, SA_{Cu} can be calculated in m^2g^{-1}. This method has to be applied carefully, as for instance too high temperatures may cause a significant extent of bulk oxidation, which leads to an overestimation of SA_{Cu} [41,42]. Also reaction of oxygen vacancies of the oxide components with N_2O or modified reactivity of a defective Cu surface towards N_2O may be a source of error. SA_{Cu} of the state-of-the-art methanol synthesis catalyst measured by this method amounts to 25-35 m^2g^{-1}. If reliable data of the average Cu particle size are available, e.g. by sufficient TEM observations [39], the degree of oxide coverage of the Cu particles, i.e. the average ratio of interface to surface area, can be calculated. For industrial $Cu/ZnO/Al_2O_3$ catalysts, this value is around 35% [43]. The high MSR activity of this type of $Cu/ZnO/(Al_2O_3)$ catalysts at relatively low temperatures can most likely be explained with the large SA_{Cu} due to this favorable microstructure and to the proper balance of Cu dispersion and loading.

Clearly, one role of ZnO is to act as spacer and stabilizer avoiding direct contact of the Cu particles and preventing them from sintering [44]. In addition to this geometrical function, a so-called Cu-ZnO synergy is described in literature for the methanol synthesis reaction [45]. The nature of this synergy is debated and several models have been proposed. Strong metal-oxide-interactions (SMSI) between Cu and ZnO were observed at highly reducing conditions [46] and it

was suggested that partially reduced ZnO_x migrates onto the surface of the Cu particles under methanol synthesis conditions [47]. On a supported Cu/ZnO model catalyst, reversible wetting/de-wetting was observed as the reduction potential of the gas phase was varied [48] which was not detected on Cu/SiO_2. While the role of surface decoration or morphology change for high performance catalysts under industrial methanol synthesis conditions is still unclear, a correlation of the concentration of planar defects in the Cu particles with the catalytic activity in methanol synthesis was observed in a series of industrial $Cu/ZnO/Al_2O_3$ catalysts by Kasatkin et al. [39]. Planar defects like stacking faults and twin boundaries can also be observed by HRTEM and are marked with arrows in Figure 2f. The origin of strain and defects is thought to be the interface of the Cu particles with the ZnO phase.

It is generally agreed that the role of ZnO in Cu-based methanol synthesis catalysts exceeds the function of a mere physical stabilizer and ZnO is a crucial component in high performance methanol synthesis catalysts. In light of the fact, that highly active Cu-based MSR catalysts can also be prepared in absence of ZnO (e.g. as Cu/ZrO_2, see below), this type of Cu-ZnO synergy does not seem to be an as critical factor in case of MSR compared to methanol synthesis or it is not as strictly limited to ZnO.

On the other hand, there are many similarities of methanol synthesis and MSR [35]. This is often accounted for by the concept of microscopic reversibility, as MSR formally is the reverse reaction of methanol synthesis. It has to be considered, however, that the differ-

ent reactant gas mixtures used for MSR and methanol synthesis will affect the surface state of the catalyst, which consequently will be different under highly reducing methanol synthesis conditions compared to the much less reducing MSR feed. Thus, unlike forward and backward reactions at equilibrium, methanol synthesis and MSR probably take place over practically different catalytic surfaces. This general limit of the application of the concept of microscopic reversibility has been pointed out by Spencer for WGS and rWGS [49] and is valid accordingly also for methanol synthesis and MSR [50]. One may conclude that an optimized methanol synthesis catalyst, for which the fine tuning of preparation and operation conditions is far more advanced, will also be active in MSR due to its generally large SA_{Cu} and represents a powerful reference system, but it does not necessarily represent the optimal catalyst for this reaction [50]. Finding Cu/ZnO/X systems with a composition and microstructure optimized for the MSR reaction is thus the major current challenge in development of a MSR catalyst for energy applications.

Drawbacks of Cu/ZnO-based catalysts

The unique microstructure of modern Cu/ZnO/(Al_2O_3) methanol synthesis catalysts described above is responsible for many advantages of Cu-based catalysts and their application in MSR, such as high SA_{Cu}. However, a major drawback of Cu-based catalysts is their lack in long-term stability.

A loss of 30-40% of the initial MSR activity was observed by Frank et al. [38] for a selection of Cu-based catalysts in combination with

different oxide components (Fig 3d). Deactivation proceeds fast during the first 100 hours on stream and tends to level off afterwards. Deactivation of $Cu/ZnO/Al_2O_3$ catalysts in MSR has been reviewed by Twigg and Spencer [50]. A major aspect is the loss of SA_{Cu} due to Cu particle sintering. The melting point of elemental Cu is relatively low at T_M = 1336 K resulting in low Tamann and Hüttig temperatures of 0.5 T_M and 0.3 T_M, respectively. The former refers to the approximated onset temperature of atom mobility leading to thermal sintering, while the latter is estimated to be the onset temperature of defect annealing. Compared to other metals, Cu is generally quite sensitive to sintering [51] and, as a rule of thumb, Cu-based catalysts should not be operated above ca. 600 K after activation. For the same reason, also the pre-treatment conditions of the catalysts have to be selected with care. Especially the exothermic reduction step during catalyst activation is crucial, as the heat of reduction may cause high local temperatures, thermal sintering and a loss of SA_{Cu}. In spent Cu-rich commercial methanol synthesis catalysts intermediate stages of sintering by coalescence can be identified by HRTEM (Fig. 3a,b) [52]. Interestingly, the formation of five-fold cyclic twins originating from the contact area of two Cu particles is observed in these images. The evolution of the Cu particle size distributions (Fig. 3c), determined by evaluation of TEM micrographs of several thousand Cu particles, shows a clear widening and shift of the particle size distribution to larger particle diameters.

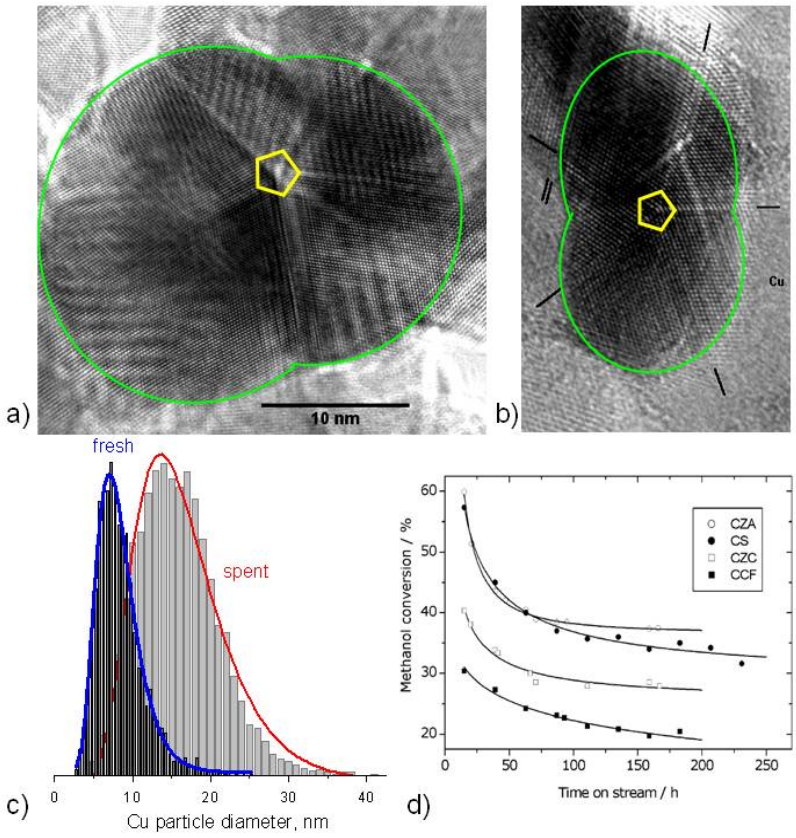

Fig. 3: HRTEM images of $Cu/ZnO/Al_2O_3$ catalyst used in methanol synthesis (a,b); evolution of the particle size distribution during reaction (c); and loss in methanol conversion with time on stream for different Cu-based catalysts during MSR at 493 K, 1 bar, $MeOH:H_2O$ = 1:1 (d, CZA: 0.5g $Cu/ZnO/Al_2O_3$, CS: 2.0g Cu/SiO_2, CZC: 1.0g $Cu/ZrO_2/CeO_2$, CCF: 2.5g $Cu/Cr_2O_3/Fe_2O_3$, Reprinted from ref [38] with permission from Elsevier)

Rapid deactivation is not only caused by external heat input during reaction alone, also the operating atmosphere of the catalyst has to be considered. In methanol synthesis, which is operated at a similar temperature like MSR, modern $Cu/ZnO/Al_2O_3$ catalysts can deliver stable performance over years on stream. The same catalyst may tend to deactivate more rapidly under MSR conditions suggesting a critical role of the gas phase composition, most probably of water in

the feed, on the sintering behavior. Löffler et al. [53] investigated the stability of several commercial WGS catalysts in the MSR reaction and fitted their data using a sintering model. $Cu/ZnO/Al_2O_3$ formulations were found to be most active compared to other catalyst compositions, but were also most prone to deactivation by sintering. In their analysis of catalyst deactivation of a commercial $Cu/ZnO/Al_2O_3$ catalyst during MSR, Thurgood et al. [54] revealed that in addition to the loss of surface area, also the site concentration at the catalyst's surface declined with time on stream.

The sensitivity of a given Cu/ZnO/X catalyst towards sintering under MSR conditions is determined by three main aspects: Composition (Cu:Zn ratio), nature of promoting oxide X, and catalyst microstructure. Obviously, a high Cu:Zn ratio will lower the distance between neighboring Cu particles and favor formation of direct contacts leading to sintering by particle coalescence. Lowering the Cu loading increases the stabilizer-to-metal ratio, and is thus expected to contribute to the stabilization of Cu particles. It is, however, usually not desired to significantly decrease the amount of active metal in a Cu/ZnO catalyst. In particular, it is noted that for preparation of the porous Cu-ZnO arrangement (Fig. 2) the Cu:Zn ratio is a crucial parameter, which has a clear optimum depending on the solid state chemistry of the hydroxycarbonate precursor phase and cannot be varied freely without sacrificing SA_{Cu} and, thus, activity (see below).

It seems much more promising to try to stabilize a Cu/ZnO catalyst at a given (optimized) Cu:Zn ratio by adding a second oxidic species

X and thus modify the Cu-ZnO interactions. In case of the methanol synthesis catalyst, these interactions seem to be significantly strengthened by addition of small amounts of Al_2O_3 [50]. Ternary $Cu/ZnO/Al_2O_3$ catalysts are significantly more stable towards thermal sintering and consequently show a considerably longer lifetime in methanol synthesis than binary Cu/ZnO systems. In MSR also the hydrothermal stability of the oxide phase and its contact to the Cu particles has to be considered. Looking at Figure 2e it is obvious that not only thermal sintering induced by mobility of Cu, but also segregation or re-crystallization of the ZnO component (e.g induced by steam) will have the same detrimental effect on the porous Cu/ZnO arrangement and cause a loss of SA_{Cu}. Other ZnO/X combinations than ZnO/Al_2O_3, especially ZnO/ZrO_2 (see below) are promising candidates for preparation of improved Cu-based MSR catalysts.

The third important consideration concerns the microstructure of the catalyst and is closely related to the Cu:Zn ratio and to the stabilizing interactions between Cu metal and the oxide. Modern $Cu/ZnO/Al_2O_3$ catalysts exhibit a unique and apparently fragile microstructure. The nano-scaled arrangement of metallic Cu and oxidic spacer particles seen in Figure 2 is metastable and an irreversible gradual breakdown of the porous aggregates can be expected if the sample is submitted to thermal stress as the system lowers its free surface energy. Highly active $Cu/ZnO/Al_2O_3$ is pyrophoric and may even deactivate upon contact to air as the heat of oxidation of the highly reactive Cu nanoparticles is sufficient to cause sintering. A microstructure exhibiting larger and more stable Cu-ZnO interfaces

may thus be desirable in order to stabilize the Cu particles. It is noted that the catalyst's microstructure heavily depends on its preparation history [17]. For example, at a given industrially relevant composition (Cu:Zn:Al = 60:25:15) the interface-to-surface ratio can be significantly increased to 50% for a $Cu/ZnO/Al_2O_3$ catalyst, if the precursor preparation is modified by going from a batch process including precipitate ageing to a continuous process suppressing the ageing period [43]. In this example, the Cu particles have a similar size like in a conventional $Cu/ZnO/Al_2O_3$ catalyst, but are more deeply embedded into an amorphous oxide matrix and modified Cu-oxide interactions can be expected (Fig. 4). Generally, a low value of the interface-to-surface ratio of the Cu particles enables a large SA_{Cu}, while a larger value leads to stronger embedment and different wetting behavior which may increase the stability of the catalyst towards thermal sintering. An intermediate value may represent a kind of compromise between both effects.

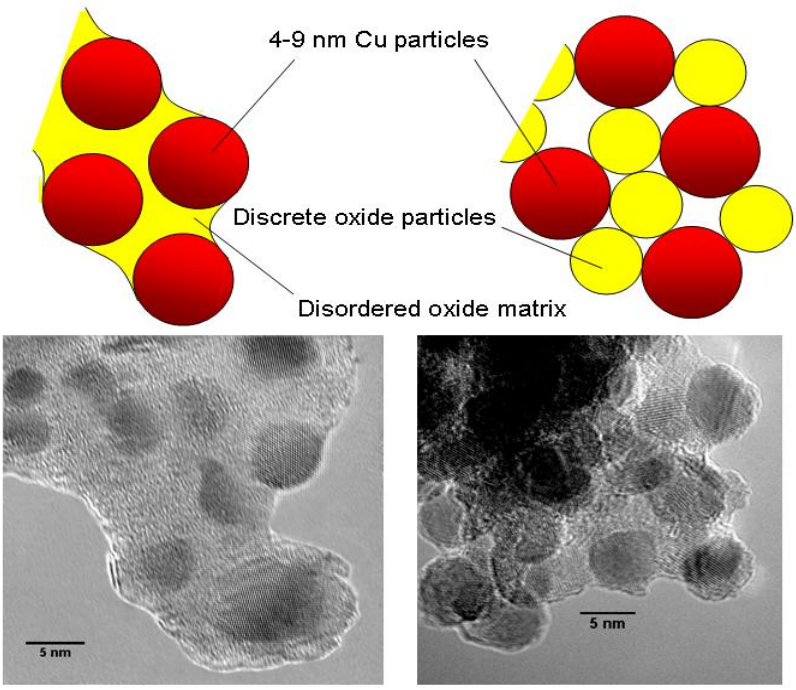

Fig. 4: Scheme and TEM micrographs of the microstructure of differently prepared $Cu/ZnO/Al_2O_3$ catalyst with the same composition and similar Cu particle sizes; adopted from ref [43].

Other sources of catalyst deactivation are catalyst poisons like sulfur or chlorine [50]. These contaminations do typically not originate from the methanol feed, but may be present in steam or air used for MSR or oxidative MSR. Sulfur acts as a site blocking poison for Cu and chlorine promotes sintering by formation of low-melting and mobile Cu and Zn chlorides. Agarwal et al. [55]. reported coke formation as another source of deactivation of $Cu/ZnO/Al_2O_3$ catalysts in MSR.

The other major problem of Cu-based MSR catalysts is the formation of still too much CO during MSR, typically in the low %-

range. Agrell et al. [56] reported that the problem of CO formation over $Cu/ZnO/Al_2O_3$ catalysts can be attenuated by increasing the steam-to-methanol ratio or by the addition of oxygen or air (oxidative MSR). CO is formed at high methanol conversions most likely by the rWGS reaction consecutively to MSR as a secondary product. Decreasing the contact time leads to lower CO selectivity. Lowering the reaction temperature is also helpful as it disfavors the rWGS equilibrium. Thus, probably the best way to make a Cu-based MSR catalyst less selective to CO would be to make it more active at lower temperatures.

Preparation of Cu/ZnO-based catalysts

The most studied member of the Cu/ZnO catalysts family for C1 chemistry is the commercial methanol synthesis catalyst, which can be seen as a reference system for Cu-based MSR catalysts (see above). It is prepared by co-precipitation, which is by far the most important method for synthesis of Cu/ZnO-based catalysts.

The industrially applied preparation of the low-temperature methanol synthesis catalyst was introduced by ICI company in 1966 and comprises co-precipitation and ageing of a mixed Cu,Zn,(Al) hydroxy-carbonate precursor material, thermal decomposition yielding an intimate mixture of the oxides and finally activation of the catalyst by reduction of the Cu component [57]. The synthesis parameters have been studied in many academic and industrial groups and a high degree of optimization could be achieved over the last decades by mostly empirical fine-tuning of the conditions. The delicate na-

noparticulate and porous microstructure of the industrial methanol synthesis catalyst (see above) can only be obtained if the optimized parameters are strictly obeyed during synthesis. Especially the synthesis conditions during the early co-precipitation and ageing steps turned out to be crucial for the catalytic properties of the resulting methanol synthesis catalyst. This phenomenon, sometimes termed the "chemical memory" of the Cu/ZnO system [58], indicates the critical role of the preparation history of this catalyst system [17,59,60]. As was already mentioned above and is obvious form Figure 2, the microstructural arrangement of Cu and ZnO in the final catalyst is metastable and tends to lower its free energy by sintering and segregation into macroscopic crystallites. Considering that the desired composite product is thus only kinetically stabilized and does not represent a deep minimum in the free energy landscape, it is not surprising that the precursor, i.e. the starting point of our path through the energy landscape during preparation, is of decisive importance for the exact position of our end point at which we wish to kinetically trap the system to obtain the arrangement like seen in Figure 2. Baltes et al. [59] elaborated a quantitative basis of the chemical memory in a systematic study and reported dramatic difference in SA_{Cu} of $Cu/ZnO/Al_2O_3$ catalysts of the same composition as pH or temperature of the co-precipitation step was varied. If self-made Cu/ZnO catalysts are employed as reference systems for MSR studies, it is thus very important to carefully prepare the catalyst as it is much easier to synthesize a poor Cu/ZnO catalyst than a good one,

which could act as a conclusive reference for comparison with novel materials.

Preferred Cu:Zn ratios for ternary Cu,Zn,Al and binary Cu,Zn catalysts are near 70:30 [61] or 2:1 [62]. It was reported that the best catalysts can be obtained by constant pH co-precipitation with Na_2CO_3 solution at pH 6 or 7 and at elevated temperatures around 333 – 343 K [59,63]. Ageing of the initial precipitate is crucial [62,64,65] and takes from around 30 min to several hours. Calcination is typically performed at relatively mild temperatures around 600 – 700 K. No doubt, this multi-step preparation of Cu/ZnO catalysts is complex, but some progress in understanding the chemical memory has been made recently and helps to rationalize the benefit of exactly this setting of parameters.

It is clear that the target microstructure shown in Figure 2 requires a homogeneous and maximized intermixing of the Cu and Zn species in order to stabilize the alternating arrangement of small Cu and ZnO nanoparticles. Thus, the main goal of the preparation is to carry over and maintain the perfectly homogeneous cation distribution in the mixed solution to a maximum extent via the precipitate to the final catalyst. The first step in this process is the solidification of the dissolved Cu and Zn cations by precipitation by elevation of pH. Precipitation titration is an elegant way to study the cation hydrolysis of Cu^{2+} and Zn^{2+} under conditions relevant for catalyst preparation [66]. Such experimental results are shown in Figure 5a-c.

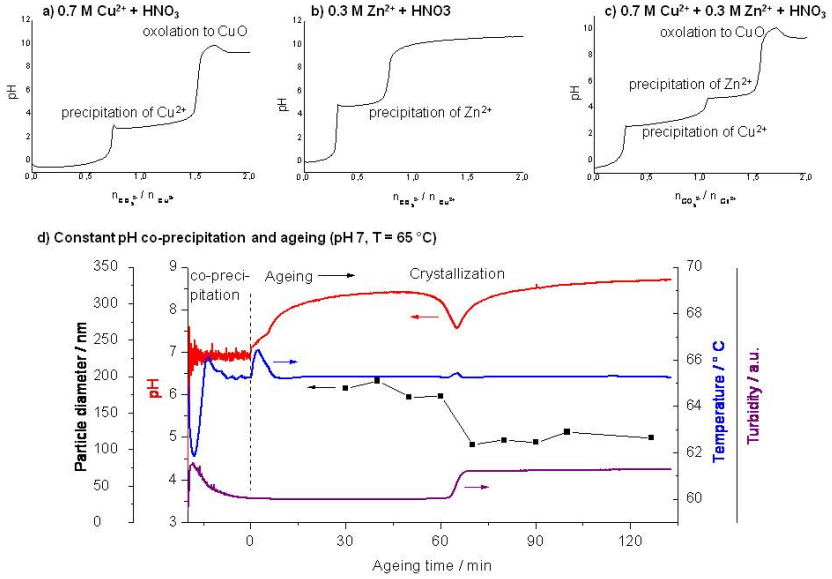

Fig. 5: Precipitation titration curves relevant for the co-precipitation of $Cu/ZnO/Al_2O_3$ catalyst precursors at 338 K using aq. Na_2CO_3 as precipitation agent (a-c, adopted from ref. [66]); preparation log of corresponding constant pH co-precipitation, adopted from ref. [67] (d).

It can be seen in Figure 5a that the hydrolysis of the pure Cu^{2+} solution is characterized by an underlying neutralization of the acidic starting solution with the basic precipitating agent. The S-shaped neutralization curve is interrupted by a precipitation plateau near pH 3, where Cu^{2+} forms a precipitate. If we now look at the Zn^{2+} solution (Fig. 5b), a qualitatively similar picture emerges, but with the important difference that the Zn-precipitate is formed at pH 5 instead for pH 3. Such differences in hydrolysis behavior are of course not uncommon and are the basis for the traditional wet chemical ion separation techniques used for qualitative cation analysis. What is important, however, is that the precipitation titration curve of the binary system (Fig. 5c) is directly composed of those of the single sys-

tems. This fact indicates that there is no formation of a mixed binary precipitate under these conditions, but that Cu^{2+} is first completely precipitated at pH 3, which can be also seen from the vanishing of the blue color from the mother solution at pH 4, while Zn^{2+} is precipitated "on top" later at pH 5. Clearly, such increasing pH processes cannot yield a well intermixed precipitate. The solution to this problem is the application of the constant pH co-precipitation technique [68,69], meaning that the acidic metal solution and the precipitating agent are dosed simultaneously in a way that the average pH in the reaction vessel is maintained more or less constant. Using this mode of precipitation, it is possible to precipitate Cu and Zn very close in space and time as the curves shown in Figure 5 are passed through not for the whole batch at once, but for every single droplet that hits the receiver solution. Thus, the cation distribution in the precipitate obtained by constant pH co-precipitation is much more homogeneous [66].

Also the suitable pH for the precursor preparation can be deduced from the titration curves shown in Figure 5. It should not be lower than pH 5 to guarantee complete precipitation of Zn^{2+} (and Al^{3+}), which otherwise would remain at least partially in solution. On the other hand, the pH should stay below pH 9, because in a very basic solution de-mixing of the Cu,Zn precipitate by oxolation of basic copper precipitates into stable tenorite, CuO, occurs [66]. This oxolation can be seen as a dip in the titration curves at high pH. Indeed, CuZn(Al) precursors are typically co-precipitated at neutral or even slightly acidic pH [59,62,63]. It is noted that the position of the pre-

cipitation plateaus are also a function of temperature [66]. An increase in temperature of co-precipitation leads to a shift of the titration curves to lower pH values confirming that the proper selection of pH *and* temperature is crucial to guarantee the rapid and complete solidification of all components. Thus, pH 6–7 can only be regarded as optimal within a certain temperature window of 333–343 K [59,66].

The initial Cu,Zn precipitate obtained by constant pH co-precipitation undergoes important changes during stirring in the mother liquor. This ageing process is associated with crystallization, a change in color from blue to bluish green and a change in particle size and morphology (Fig. 6d) [67]. Ageing critically affects the micro-structural as well as the catalytic properties of the resulting Cu/ZnO catalyst [70]. These changes occur rather step-like than gradually and are accompanied by a transient minimum in pH. The phase composition of the ageing product is mostly determined by the Cu:Zn ratio [60,72], but also by the mode of precipitation [72], and the speed of addition of the precipitating agent [73]. Typical phases obtained when going from Cu-rich to Zn-rich compositions are malachite $Cu_2(OH)_2CO_3$, zincian malachite $(Cu,Zn)_2(OH)_2CO_3$ (sometimes called rosasite, see ref. [74]), aurichalcite $(Cu,Zn)_5(OH)_6(CO_3)_2$, hydrozincite $Zn_5(OH)_6(CO_3)_2$ and mixtures thereof. In ternary Cu,Zn,Al systems, also small amounts of layered double hydroxides may be observed. This precursor phase is covered in detail in the next section. Due to the homogeneity ranges of the mixed phases, a comprehensive characterization of the precursor is

difficult. Zincian malachite was suggested to be the relevant precursor phase for industrial catalysts [62], which is also confirmed by the industrially applied Cu-rich composition near Cu:Zn = 70:30, falling into the regime in which zincian malachite is the main product.

This view could be recently confirmed by a positive correlation of the Zn-content in zincian malachite and the SA_{Cu} of the resulting catalyst [67]. The Zn fraction can be estimated from the angular position of the characteristic $(20\,\bar{1})$ XRD peak of the zincian malchite phase near 32 ° in 2θ using Cu K_α radiation [72]. This particular lattice plane distance contracts as Zn^{2+} is incorporated into zincian malachite and the corresponding peak is shifted to higher angles. This is due to the average lowering of Jahn-Teller distortions of the MO_6 building units in zincian malachite, whose elongated axes are aligned nearly perpendicular to this orientation. It is thus possible to measure the Zn-content of this phase by conventional XRD despite the similar ionic radii and scattering factors of Cu and Zn. It is noted that due to the anisotropic contraction of the monoclinic unit cell the other strong XRD peaks at lower angles, which are often employed for phase identification, are only hardly affected by Cu,Zn substitution and do not give much diagnostic insight [74]. The decrease of the $(20\,\bar{1})$ lattice plane distance upon incorporation of Zn into malachite was measured for catalyst precursor phases obtained after ageing of precipitates with different nominal Cu:Zn ratio (Fig. 6) [67]. It can be seen that, under the conditions applied in this study, the limit of Zn incorporation is found near 28%, i.e. at a composition close to

$(Cu_{0.72}Zn_{0.28})_2(OH)_2CO_3$. For higher nominal Zn content no further shift of the $(20\,\bar{1})$ reflection and crystallization of the Zn-richer aurichalcite phase as a side-product were observed. The largest SA_{Cu} is observed for catalysts prepared from precursors near this critical composition (Fig. 6). This result strongly suggests that the desired porous microstructure of Cu/ZnO catalysts (Fig. 2) is formed from highly substituted zincian malachite precursors, and that the applied Cu:Zn ration near 70:30 is beneficial, because it lies near the incorporation limit of Zn in the malachite phase.

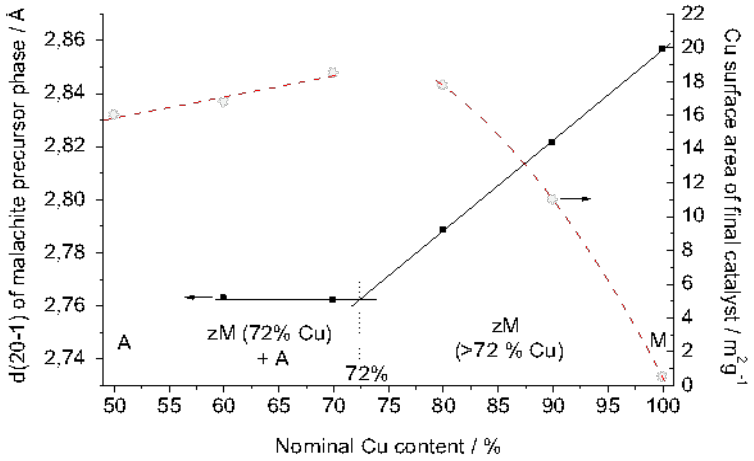

Fig. 6: Lattice contraction in the direction perpendicular to the $(20\,\bar{1})$ planes of zincian malachite as a measure of Zn incorporation in the precursor phase and SA_{Cu} of the final Cu/ZnO catalyst as a function Cu content (Phase composition: M: malachite; zM: Zincian malachite; A: Aurichalcite); adopted from ref. [67].

This insight results in a simple geometrical model for the preparation of industrial Cu/ZnO catalysts comprising subsequent meso- and nano-structuring of the material (Fig. 7) [67]. In a first micro-

structure directing step (meso-structuring) the homogeneous Cu,Zn precipitate obtained by constant-pH co-precipitation crystallizes in form of thin needles of zincian malachite. Thin and interwoven needles are desired, because the porosity of the final catalyst is already pre-determined at this step. In a second step, the individual needles are decomposed into CuO and ZnO and pseudo-morphs of the precursor needles can be still observed after mild calcinations [59]. Because both phases are only poorly miscible, a de-mixing cannot be avoided at this stage and nano-particles of the oxides, CuO and ZnO, are formed. The effectiveness of this nano-structuring step depends critically on the Zn-content of the precursor. The closer we approach a 1:1 ratio of Cu^{2+} and Zn^{2+} in the zincian malachite phase, the smaller the newly formed oxide particles will be and the higher is the dispersion of the Cu phase [67]. A 1:1 ratio of Cu and Zn in synthetic zincian malachite, however, seems to be inaccessible by conventional co-precipitation and ageing and due to solid state chemical constrains the limit is near 70:30 [74]. If we leave aside the synergetic effects of Cu and ZnO at this moment, the general benefit of using Zn^{2+} for the preparation of highly dispersed Cu-based catalysts is a geometric effect due to the chemical similarity of Cu^{2+} and Zn^{2+} concerning cation charge and size in aqueous solutions and in the precursor state. This similarity enables a common solid state chemistry of Cu and Zn in one mixed precursor phase, may it be produced by co-precipitation or impregnation. Thus, highly intermixed precursors can be prepared easily in the Cu-Zn system, leading to highly dispersed Cu and ZnO particles upon decomposition.

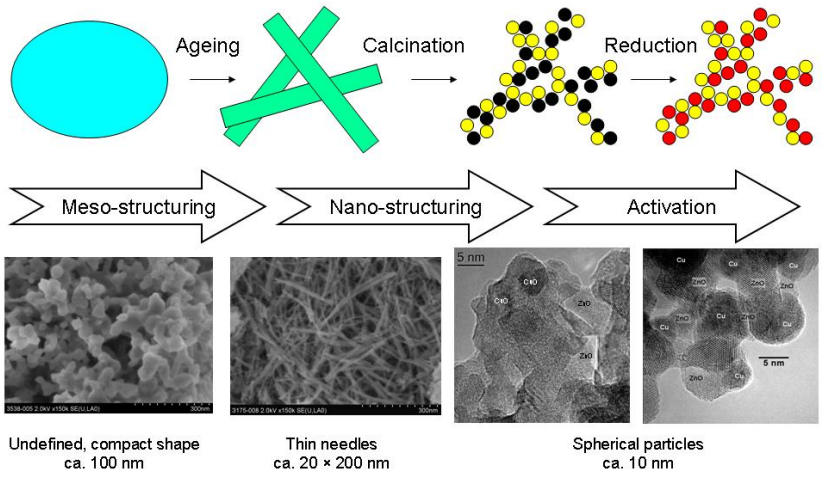

Fig. 7: Model for the chemical memory of Cu/ZnO/(Al_2O_3) catalyst preparation comprising two microstructure directing steps.

This model of Cu/ZnO preparation can explain the "chemical memory" of the industrial system, because the important material properties of the final catalyst like porosity and dispersion are already pre-determined by the properties of the precursor phase, like needle thickness and degree of Zn incorporation. It is also clear from this model that the synthesis conditions for industrial methanol synthesis catalysts were optimized in an unintended manner in order to improve the Zn incorporation into the zincian malachite precursor phase. This of course means that preparation of Cu/ZnO catalyst from other precursor phases requires a new and adjusted set of preparation conditions. The 70:30 ratio represents the optimal compromise between loading and dispersion of Cu only for catalysts prepared from zincian malachite precursors and each other precursor or preparation method requires an own optimization of the Cu:Zn ratio

(and all other synthesis parameters). Catalysts of lower Cu:Zn ratio than 70:30 are often used for MSR. This usually leads to formation of the aurichalcite precursor phase instead of zincian malachite during co-precipitation of the precursor [58,71,75]. Aurichalcite crystallizes in form of platelets rather than needles [64] and yields a Cu/ZnO catalyst of different microstructure. SA_{Cu} usually is lower [61,67], but the embedment and Cu-ZnO interactions may be more favorable for MSR. In contrast to zincian malachite, for aurichalcite, which usually does not require an extended ageing period to crystallize, a homogeneous co-precipitation method using urea decomposition has been reported to lead to highly active Cu/ZnO MSR catalysts [76,77]. Promoting oxides – Al_2O_3 in case of the industrial catalyst – usually have a higher charge than Cu^{2+} or Zn^{2+} and in case of M^{3+} ions layered double hydroxides are very interesting for formation of $Cu/ZnO/Al_2O_3$ catalysts from a single precursor phase. Also for academic purposes it is generally desirable to prepare a Cu/ZnO-based catalyst from single-phase hydroxy-carbonate precursor to obtain a homogenous microstructure, which enables drawing reliable conclusions regarding the intrinsic activity of differently prepared Cu phases.

It is noted that $Cu/ZnO/(Al_2O_3)$ catalysts active in MSR can also be prepared from other precursors than hydroxy-carbonates, like mixed oxalates, [78] or following other recipes than co-precipitation, like reactive grinding [79] or CVD [80]. All these approaches will lead to different $Cu/ZnO/(Al_2O_3)$ catalytic materials, which have to proof their performance in comparison with the high-SA_{Cu} industrial refer-

ence catalysts. It is crucial to combine such comparative catalytic studies with comprehensive material characterization to establish structure-performance relationships and to learn about possible routes to further optimize the Cu/ZnO/(Al_2O_3) system for application in MSR.

Ternary Cu/ZnO/X catalysts (X = Al_2O_3, ZrO_2)

In contrast to the widely studied and debated role of ZnO, which can be separated into a geometric (spacer function) and an electronic (synergetic Cu-ZnO interactions) contribution (see above), only very little is known about the origin of the beneficial role of Al_2O_3. Its presence leads to an improved thermal stability and higher intrinsic activity in methanol synthesis [50,81] and Al_2O_3 can be regarded as a structural promoter. As a porous oxide, alumina also provides a high surface area, but as mentioned earlier, cannot be seen as a classical support in commercial Cu/ZnO/Al_2O_3 catalysts. Many other oxides have been tested to find Cu/ZnO/X systems with improved catalytic properties, e.g. by combinatorial approaches [82]. In the field of MSR catalysts, Breen and Ross [83] compared a number of Cu/ZnO/X materials (X = Al_2O_3, ZrO_2, La_2O_3, Y_2O_3) of different composition and prepared by different precipitation sequences. They concluded that ZrO_2 is superior to Al_2O_3 as an oxide component in Cu/ZnO-based MSR catalysts. In addition to these Cu/ZnO/ZrO_2 catalysts, also Cu/ZnO/Al_2O_3 composites prepared from layered double hydroxide precursors will be discussed in this section, since their microstructure and composition is markedly different from the

commercial low-Al_2O_3 promoted Cu/ZnO system described above. It is noted that also other oxides than Al_2O_3 or ZrO_2 like for instance SiO_2 [84], and also carbon [85,86] were used to prepare active Cu/ZnO MSR catalysts.

Layered double hydroxides (LDHs) or hydrotalcite-like compounds are hydroxy-carbonate precursors, which can be derived from the naturally occurring Mg-Al salt hydrotalcite, $Mg_{1-x}Al_x(OH)_2(CO_3)_{2/x} \cdot m\ H_2O$ ($0.25 < x < 0.40$). Mg and Al form layers of edge-sharing $(Mg,Al)(OH)_6$ octahedra. The H-atoms point to the interlayer space, where also the carbonate anions are located. Carbonate ions (or other anions) are needed in the structure to compensate for the extra positive charge introduced by the trivalent Al^{3+} ions. LDHs are well-established precursor compounds for synthesis of various catalysts [87,88]. They are especially interesting due to their ability to isomorphously substitute Mg^{2+} as well as Al^{3+} by other bi- or trivalent cations, in particular those from the first row of transition metals. Thus, they are very attractive precursors for Cu-Zn-Al catalysts as they can provide a perfect atomic distribution of all metal species in one single-phase precursor compound and should yield structurally uniform catalysts of high Cu dispersion and enhanced interaction between Cu metal and the Zn,Al oxide phase.

Several studies have shown that Cu,Zn,Al LDH precursors or precursor mixtures containing the LDH phase can indeed be decomposed into highly active MSR catalysts [18,89,90]. LDHs are typically and most easily prepared by co-precipitation, similar to the zincian malachite precursor of the methanol synthesis catalyst (see

above). Preparation of phase-pure Cu,Zn,Al LDHs requires a modified metal composition with an increase in Al and a decrease in Cu content. The former is necessary to provide enough trivalent cations, which should exceed around ¼ of the total metal cations. Thus Al cannot be regarded as a structural promoter phase any more, but rather is an integral component of the oxide phase in the final catalyst. The latter is to suppress formation of Cu-rich malachite-like phases (desired in case of the industrial methanol synthesis catalyst), which is favored by Cu^{2+} due to the tendency of the d^9 system to crystallize in Jahn-Teller distorted 4+2 coordination rather than in the more regular LDH environment. Usually, no extended ageing period is needed to crystallize LDH phases from the precipitate.

Cu-rich phase-pure LDH precursors (up to 49 at.-% Cu) can be prepared by such a modified direct co-precipitation and yield $Cu/ZnAl_2O_4$-type catalysts [91]. These catalysts exhibit a different microstructure than that of the industrial $Cu/ZnO/Al_2O_3$ catalyst shown in Figure 2. Despite a smaller average Cu particle size observed in the ex-LDH material, which is a result of the lower total Cu content and the perfect cation distribution in the precursor, the accessible Cu surface area is considerable lower, around 5 m^2g^{-1}. This is a result of the much stronger embedment of the small metal particles in the $ZnAl_2O_4$ matrix. After calcinations at 603 K and reduction, the interface-to-surface ratio was determined to be 89% compared to ca. 35% for the industrial system. The major challenge in the preparation of such ex-LDH $Cu/ZnAl_2O_4$ catalyst can thus be seen to optimize the “nuts-in-chocolate”-like morphology by adjust-

ing the Cu particle size, the degree of embedment and the precursor platelet thickness in order to find the proper compromise between Cu metal-oxide interactions and Cu dispersion. Tang et al. [89] reported a surprisingly high accessible SA_{Cu} of 39 m^2g^{-1} for a LDH-derived $Cu/ZnO/Al_2O_3$ catalyst (Cu:Zn:Al = 37:15:48) after calcination of the precursor at elevated temperature of 873 K associated with the crystallization of spinel-type oxides and the complete decomposition of all carbonate on the sample. A microemulsion approach for the precipitation of the precursor to "nano-cast" the platelet morphology of the LDH phase has also been shown to be promising in this direction as it increases SA_{Cu} from 8 to 14 m^2g^{-1} compared to a conventionally co-precipitated ex-LDH $Cu/ZnAl_2O_4$ catalyst (Cu:Zn:Al = 50:17:33) [92]. The MSR activity was improved, but did not scale linearly with SA_{Cu} and was still lower compared to a commercial $Cu/ZnO/Al_2O_3$ catalyst of the type described above.

Highly active ex-LDH $Cu/ZnO/Al_2O_3$ catalysts have been reported by Turco et al. [16,93,94] The authors applied a homogenous precipitation method of the chloride containing LDH followed by anion exchange with carbonate and investigated the structural and catalytic properties of the resulting catalysts. Calcination at 723 K leads to formation of CuO, ZnO, amorphous Al_2O_3 and probably also Cu and Zn aluminates. Cu contents were between 5 and 45% of all metal ions and SA_{Cu}s of up to 17.5 m^2g^{-1} could be achieved. The highest activity in oxidative MSR was observed for the composition Cu:Zn:Al = 18:33:49. This sample sample showed a conversion to

CO near the detection limit of 0.01 %, which did not increase significantly with temperature between 473 and 673 K.

Velu at al. [18,95] have prepared Cu,Zn,Al-LDH precursors by co-precipitation and calcined at 723 K to obtain $Cu/ZnO/Al_2O_3$ catalysts. Among these, the sample of the molar composition Cu:Zn:Al = 33:43:24 showed the highest Cu dispersion. The high activity in oxidative MSR was stable over 25 h on stream. The authors also used ZrO_2 as a replacement for Al_2O_3 and as an additive to the $Cu/ZnO/Al_2O_3$ system. These $Cu/ZnO/ZrO_2$ and $Cu/ZnO/Al_2O_3/ZrO_2$ catalysts were prepared from aurichalcite and mixed aurichalcite/LDH precursors, respectively. The samples containing ZrO_2 were more effective in oxidative MSR than the ZrO_2-free samples. Copper-zirconia interactions, in particular Cu-O-Zr bonding, was found in these materials [96,97]. Cu was easier to reduce in the presence of ZrO_2 suggesting an effect of the promoter oxide on the redox-chemistry of Cu. A Cu-ZrO_2 synergetic effect was proposed to be responsible for the better catalytic performance of the ZrO_2-containing samples probably by adjusting the Cu^0/Cu^+ ratio under working conditions (see below). Such an effect of the presence of ZrO_2 on the ratio of $Cu^0/Cu^{oxidized}$ at the catalyst surface was previously suggested by Breen and Ross on basis of modified redox-chemistry of Cu detected by temperature programmed reduction (TPR) [98]. Interestingly, a decreased reducibility of Cu was observed for their ZrO_2-containing catalysts and ascribed to the presence of the promoter. The authors observed in their study that $Cu/ZnO/ZrO_2$ catalysts were more active than $Cu/ZnO/Al_2O_3$ and

the material could be further improved by addition of alumina and yttria. The interactions between Cu metal and zirconia are discussed in more detail below for ZnO-free Cu/ZrO_2 catalysts.

Agrell et al. [15] prepared and characterized several Cu/ZnO catalysts without and with addition of Al_2O_3 and/or ZrO_2 by co-precipitation and used them in MSR. Among these samples, the ZrO_2-containing systems showed the highest Cu dispersions and best MSR performances. The $Cu/ZnO/ZrO_2/Al_2O_3$ catalyst also showed a high stability in POM activity upon redox cycling compared to the binary Cu/ZnO sample, suggesting again an influence of ZrO_2 on the redox properties of Cu.

Matsumura and Ishibe [99] used $Cu/ZnO/ZrO_2$ for high temperature MSR at 673 K and compared it to binary Cu/ZnO and Cu/ZrO_2 (all 30 wt.-% CuO after calcination). They observed an increased BET surface area and smaller particles in their $Cu/ZnO/ZrO_2$ sample compared to binary Cu/ZnO. The catalytic activity was more stable than that of a commercial $Cu/ZnO/Al_2O_3$ catalyst. Interestingly, deactivation was found to be accompanied by the growth of the oxide particles rather than by Cu sintering.

An activity-promoting role of ZrO_2 was also reported by Jones and Hagelin-Weaver in a series of Cu/ZnO/X catalysts (X = ZrO_2, CeO_2, Al_2O_3) prepared by impregnation [100]. The best sample was a $Cu/ZnO/ZrO_2/Al_2O_3$ catalyst, which was most active and showed lowest CO selectivity. This catalyst was prepared by co-impregnation of Cu and Zn onto a mixture of zirconia and alumina

nanoparticles and the good catalytic properties were related to the presence of the monoclinic polymorph of ZrO_2.

ZnO-free Cu-based catalysts

Among the ZnO-free Cu-based catalysts, those comprising ZrO_2 and CeO_2 are the most studied systems and will be in the focus of this section. Combinations of Cu with chromia [101-103], or manganese oxide [101] promoters or Cu on silica supports [104] have also been used in MSR. Depending on the Cu content and the method of preparation – co-precipitation, sol-gel chemistry or impregnation – these catalysts can be either obtained in form of truly supported or bulk catalysts similar to the industrial $Cu/ZnO/Al_2O_3$ system. Also skeletal Cu catalysts are known to be active in MSR, which can be prepared from Cu-containing alloys by selective leaching. These materials are prepared employing intermetallic compounds as precursor phases and are discussed in more detail in the second part of this chapter.

In the last years there has been growing interest in ZnO-free Cu/ZrO_2 as catalyst for the MSR reaction. Already in the 1980s, higher conversions of methanol were reported for Cu/ZrO_2 in comparison with Cu/SiO_2 prepared by impregnation methods [105,106]. Cu/ZrO_2 catalysts prepared by precipitation showed turnover frequencies comparable to a Cu/ZnO catalyst [98]. The lower total activity for the Cu/ZrO_2 catalysts was ascribed to lower SA_{Cu} in these catalysts. Ritzkopf et al. [20] successfully applied a microemulsion technique using the water droplets of a water-in-oil system to con-

fine the reaction space for co-precipitation. They obtained intimately mixed CuO/ZrO_2 particles with 4–16 wt.-% Cu and a particle size of less than 10 nm. At high temperature this catalyst showed activity levels identical to a commercial catalyst, but the level of produced CO was substantially reduced. At 573 K and ca. 90% conversion the CO concentration in the effluent was only ca. one fifth compared to the Cu/ZnO reference. In contrast to the commercial catalyst, oxidized Cu species were detected by X-ray photoemission spectroscopy (XPS) on the surface of the Cu/ZrO_2 catalyst after reaction, supporting the stabilizing role of ZrO_2 on oxidized Cu species, which was also observed for ZrO_2-promoted $Cu/ZnO/(Al_2O_3)$ catalysts (see above). Such oxidized Cu^+ species are discussed to play an important role in the MSR reaction (see below).

Purnama et al. [19] reported about a Cu/ZrO_2 catalyst prepared by a templating procedure (8.5 wt.-% Cu) which showed higher activity as a function of W_{Cu}/F and better stability during MSR as well as a lower production of CO compared to a commercial $Cu/ZnO/Al_2O_3$ sample. This sample showed a complex activation behavior if oxygen pulses were added to the feed after certain periods of time on stream. Szizybalski et al. [107] prepared a Cu/ZrO_2 catalyst with 8.9 mol-% Cu after calcination by a precipitation method and investigated this phenomenon more closely. The calcined catalyst contained small and disordered CuO particles rather than Cu^{2+} incorporated in to the zirconia lattice. Again, a decreased reducibility was observed. By means of *in situ* Cu K-edge X-ray absorption spectroscopy, a significant amount of residual oxygen was detected in the Cu phase

after reduction at 523 K, which could only be removed by treating the catalyst with hydrogen at 673 K. If oxygen was added to the feed during MSR, an increase of this residual oxygen concentration was detected after re-reduction in the feed, which was accompanied by an increase in MSR activity. Thus, a correlation of the amount of oxygen remaining in the copper particles and the catalytic activity was proposed leading to the conclusion that there must be a different metal support interaction of Cu/ZrO_2 compared to Cu/ZnO catalysts, where such correlation was not observed.

Similar to the Cu/ZnO system, a high Cu loading of 80 wt.-% was reported to yield the most active material if co-precipitation and nitrate solutions were used for preparation of Cu/ZrO_2 catalysts [108]. Yao et al. [109] prepared Cu/ZrO_2 catalysts with this composition by four different methods and showed that the catalysts prepared by co-precipitation revealed a higher conversion compared with the ones prepared by impregnation. The best results were obtained by an oxalate gel co-precipitation method and for a calcination temperature of 823 K [110]. In this catalyst, a thin layer of monoclinic ZrO_2 was detected on a bulk of tetragonal ZrO_2. With increasing calcination temperature the amount of monoclinic ZrO_2 increased accompanied by decreasing conversions.

Wu et al. [111] have studied the effect of ZnO and ZrO_2 on the catalytic properties of Cu in MSR by comparing pure Cu with inverse ZnO/Cu and ZrO_2/Cu model systems. Both oxides were found to enhance the activity of Cu and to stabilize the Cu particles against aggregation and sintering. Moreover, the presence of the oxides result-

ed in a stabilization of Cu^{+} species at the surface of the catalyst. The authors concluded that ZrO_2 is the superior promoter oxide for the Cu-based MSR catalyst.

Also CeO_2 turned out to be a promising oxide component for Cu-based MSR catalysts. Cu/CeO_2 catalysts were prepared by Liu et al. [21,112,113] using a co-precipitation method and calcination at 723 K. By this treatment up to 20% Cu^{2+} could be incorporated into the ceria lattice. After reduction a Cu/CeO_2 catalyst was obtained (3.9 wt.-% Cu), which was more active than Cu/ZnO and $Cu/Zn/Al_2O_3$ catalysts of the same low Cu loading. After deactivation the initial activity could be regenerated by re-calcination and reduction. The high activity was ascribed to strong Cu-oxide interactions and related to the high oxygen mobility of the ceria support. Also mixed CeO_2/ZrO_2 [114] or Zr- [115] or Gd-doped [116] ceria was used as support for Cu-based MSR catalysts.

The increasing Cu-oxide interactions when going from Cu/ZnO over Cu/ZrO_2 to Cu/CeO_2 are also reflected in a more and more enhanced substitution chemistry in the oxide phase at higher temperatures. While Zn^{2+} and Cu^{2+} show a common solid state chemistry only on the stage of the precipitated catalyst precursor, e.g. in form of a joint cationic lattice of hydroxy carbonate phases (see above), significant isomorphous substitution of Cu^{2+} in ZnO is, despite the match of cationic charge and similar ionic radii, hardly observed. The reason for this low degree of solid state solubility is most likely the tetrahedral coordination environment of Zn^{2+}-sites in ZnO, which is unfavorable for Cu^{2+}, which preferrs a Jahn-Teller-distorted octahedral

4+2 coordination. Incorporation of M^{2+} cations, like Ca^{2+}, in the zirconia lattice on the other hand is well-know and can stabilize the higher symmetric polymorphs of ZrO_2. It was reported that also Cu^{2+} can substitute Zr^{4+} and has an effect on the zirconia phase composition [117], but this effect may not play a role for preparation of Cu-based MSR catalysts, where calcination temperatures are usually low and Cu was observed to be present rather in form of highly dispersed CuO [107]. In case of CeO_2, however, clear evidence for the formation of a $Ce_{1-x}Cu_xO_2$ solid solution during catalyst preparation applying a calcination temperature of 723 K was presented by Liu et al. [21,112,113] Both materials, ZrO_2 and CeO_2, are known to easily form sub-stoichiometric metal-to-oxygen ratios and the charge mismatch upon incorporation of Cu^{2+} can be compensated by formation of oxygen vacancies. Although highly substituted bulk phases are not likely to form under MSR conditions or even in oxidative MSR atmosphere and thus themselves are probably not relevant for catalysis, these considerations still show that differences in the solid state reactivity of Cu with different oxides exist. Under oxidative conditions the systems tend to form mixed oxides by beginning oxidation of the Cu metal, while under reducing conditions the systems tend to form an alloy by beginning reduction of the oxide. The connection of the redox chemistry of the Cu phase and its interaction with the oxide component was observed by many researchers. From the substitution chemistry of the bulk oxide phases, it is understandable that ZrO_2 and CeO_2 have a stabilizing effect on oxidized Cu leading to a

higher reduction temperature, while this effect is not observed for ZnO [118].

Strengthened interactions between Cu metal and the oxide are obviously important for the stability of the catalysts as they hinder mobility of the Cu particles and thus decrease the tendency for thermal sintering. Furthermore, these interactions may be important for the accessibility of higher Cu oxidation states at given conditions, or more generally for the ease of oxygen incorporation into the Cu lattice (see below). Another practical aspect is that the re-dispersion of the Cu phase by oxidative regeneration will work much better for those systems which can form mixed oxides like Cu/CeO_2 (stronger interactions) compared to those which cannot easily form mixed phases like Cu/ZnO.

In an optimized Cu-based catalyst for MSR, the beneficial effect of redox promoting oxides on the Cu phase should be combined with the proven structural promoting effects of the less redox active ZnO/Al_2O_3 components.

The active form of Cu under MSR conditions

The question to what is the active site of Cu-based catalysts in MSR is still unclear and debated in literature. Similar to the methanol synthesis reaction either metallic Cu^0 sites, oxidized Cu^+ sites dispersed on the oxide component or at the Cu-oxide interface or a combination of both kinds of sites are discussed to contribute to the active ensembles at the Cu surface. Furthermore, the oxidic surface of the refractory component may take part in the catalytic reaction as well

as providing adsorption sites for the oxygenate-bonded species [119], while hydrogen is probably adsorbed at the metallic Cu surface.

Clearly, SA_{Cu} is among the most important factors determining the activity of a Cu-based catalyst in MSR, indicating the importance of proper balance of Cu dispersion and loading and thus of catalyst preparation. Sufficient SA_{Cu} is a prerequisite for a high performance Cu-based MSR catalyst, but the metallic Cu surface area measured by N_2O decomposition does not scale linearly with activity in all cases, and turnover frequencies - which were calculated using SA_{Cu} as a count of active sites - vary even for the same sample after different pre-treatments [120]. Thus, other factors intrinsic to the Cu phase and not detectable by the N_2O titration method also contribute to the MSR activity. There are two major views discussed in literature relating these intrinsic factors either to the variable oxidation state of Cu, in particular to the *in situ* adjustment of the Cu^0/Cu^+ ratio at the catalyst's surface, or to the defect structure and varying amount of disorder in metallic Cu depending on the microstructure and preparation history of the catalyst. As we will see, these views are not necessarily contradicting each other.

Changes of the oxidation state of Cu are to be considered in particular in oxidative MSR due to the presence of gas phase oxygen. It has been tried to answer the question of the oxidation state of Cu under (oxidative) MSR conditions by post-reaction characterization as well as by *in situ* investigations with sometimes different results depending on the feed gas compositions, the catalyst material studied and

the characterization method used. Near-surface sensitive techniques like X-ray photoelectron spectroscopy (XPS) are well-suited to investigate the oxidation state of the near-surface of a Cu-based MSR catalyst, although the discrimination of Cu^+ and Cu^0 may be challenging on basis of the core level spectra. It is noted that contact to air has to be strictly avoided to obtain reliable results as highly dispersed Cu particles are prone to oxidation in air. Another drawback is that with laboratory XPS only *ex situ* investigations are possible and potential changes of the catalyst upon cooling and evacuation have to be taken into account. X-ray diffraction and X-ray absorption spectroscopy are also widely used to characterize the Cu phase in MSR catalysts. With these methods *in situ* investigations are possible, but they lack surface sensitivity. Another general aspect to be considered when reporting $Cu^0/Cu^{oxidized}$ ratios is the homogeneity of the catalyst studied. If different Cu species are present in the catalyst, e.g. larger Cu particles as well as highly dispersed Cu clusters, additional characterization information is needed to identify the effect of the individual Cu species on the results.

Agrell et al. [15] studied the near-surface region of a $Cu/ZnO/ZrO_2/Al_2O_3$ catalyst by XPS after simulating oxidative MSR reaction conditions in the pre-treatment chamber. They reported the presence of metallic Cu^0 after reduction and formation of oxidized Cu^+ species after exposure to a O_2/MeOH atmosphere (1:2). In contrast, Goodby and Pemberton [121], who used pure MSR atmosphere without oxygen and a commercial $Cu/ZnO/Al_2O_3$ catalyst, found still about 7% Cu^+ at the surface after reduction in hydrogen,

but the catalyst was fully reduced after using it in MSR. Raimondi et al. [122] used a similar method and found that the oxidation state of Cu in a commercial $Cu/ZnO/Al_2O_3$ catalyst is a function of feed gas composition. At slightly sub-stoichiometric O_2:MeOH ratio Cu^+ was predominant only at temperatures below 510 K. At higher temperatures Cu was reduced by MeOH to its metallic state. H_2 was produced only when Cu^+ or Cu^0 were detected, while Cu^{2+} formed at higher O_2 partial pressures was inactive and led to MeOH combustion. Using a sub-monolayer Cu on thin oriented ZnO films as model catalyst the same group showed that aggregation of the Cu islands is promoted by the presence of O_2 if Cu was in the metallic state at a O_2:MeOH ratio below 0.25 at 550 K. At higher O_2 concentrations Cu is oxidized and the aggregation is less pronounced suggesting an effect of the oxidation state of Cu on the Cu-ZnO interactions [123]. Reitz at al. [124] used bulk-sensitive *in situ* X-ray absorption spectroscopy to study the oxidation state of Cu under different conditions in the presence of methanol, steam and oxygen. They observed MSR-inactive Cu^{2+} at low O_2 conversions and found H_2 production only if metallic Cu was detected. Cu^+ was detected as an intermediate during the reduction of Cu^{2+} to Cu^0.

It is not a surprise that the oxidation state of Cu is a function of the oxidation power of the gas feed, especially of the O_2 concentration if oxidative MSR is used. Knop-Gericke et al. [125] have shown the importance and complexity of the dynamic near-surface Cu-O chemistry by high pressure *in situ* XPS for the MeOH oxidation reaction on Cu foil. With increasing O_2:MeOH ratio the *in situ* formed Cu

surface could vary from metal via sub-oxide to Cu(I)-oxide like species. The most active and selective state (to formaldehyde) observed in this study was a disordered Cu^0 surface modified *in situ* by subsurface oxygen of a composition near $Cu_{\sim 10}O$ stressing that the pure Cu^0 metal and bulk Cu_2O phases are not sufficient to fully describe the surface chemistry of the Cu-O system. It is noted that the active surface phase was only observed *in situ* and did not form under UHV conditions.

It is not only the gas phase composition, which determines the oxidation state of Cu under MSR conditions. Also the catalyst formulation plays a significant role. It was already mentioned above that the presence of ZrO_2 generally decreases the reducibility of CuO and can stabilize Cu^+ compared to ZrO_2-free systems at given MSR conditions. Such Cu^+ centers are often discussed to be the active sites of (oxidative) MSR in the context of a redox-mechanism corresponding to the reverse of a reaction proposed for methanol synthesis by Klier [126], where Cu^+ centers incorporated in a ZnO matrix are suggested as active sites. The Busca group identified Cu^+ sites at the surface of LDH-derived $Cu/ZnO/Al_2O_3$ catalysts using IR spectroscopic methods and discussed their role in oxidative MSR [90,127-129].

The second explanation for a varying intrinsic activity is the different amount of disorder in the metallic Cu phase. This disorder can manifest itself in form of detectable lattice strain, e.g., by line profile analysis of XRD peaks [17], ^{63}Cu-NMR lines [65], or as an increased disorder parameter (Debye-Waller-factor) derived from extended X-ray absorption fine structure (EXAFS) spectroscopy [120].

Strained copper has been shown theoretically [130] and experimentally [131] to have different adsorptive properties compared to unstrained surfaces. Strain, i.e. local variation in the lattice parameter, is known to shift the centre of the d-band and alter the interactions of metal surface and absorbate [132]. Alternatively, a modification of the electronic structure of Cu was also discussed to take place at the interface between Cu metal and the semiconducting oxide forming a Schottky junction [133].

Günter at al. [120] used *in situ* XRD and EXAFS and found a correlation of disorder in the Cu phase and the activity of a series of differently prepared Cu/ZnO catalysts in MSR. Also the selectivity towards CO_2 was affected. Kniep et al. [65] could show that the Cu phase in Cu/ZnO catalysts prepared under otherwise identical conditions was more strained and more active in MSR if the precipitate was aged than without ageing. Also introduction of a microwave heating step [134] or reactive grinding [135] of the calcined CuO/ZnO material was used to prepare strained and disordered and, thus, intrinsically more active Cu particles in the final MSR catalyst. A certain increase in disorder seems to be also achievable by post-preparation treatment as could be shown by *in situ* investigations (Fig. 8) [120]. Addition of oxygen to the MSR feed led to a transient breakdown of MSR activity ascribed to the formation of CuO. After switching off the oxygen stream, the catalyst was re-reduced to Cu^0 in the MSR feed and exhibited a higher conversion of methanol as well as lower selectivity to CO, which was ascribed to an increase in structural disorder. Bulk-Cu_2O was observed only as an intermediate

during reduction. The origin of structural disorder in highly active Cu/ZnO catalysts is thought to be the interface of the Cu^0 clusters with the ZnO particles. Thus, enhancement of this interface contact may be beneficial for the activity of the catalyst, if not too much SA_{Cu} is sacrificed.

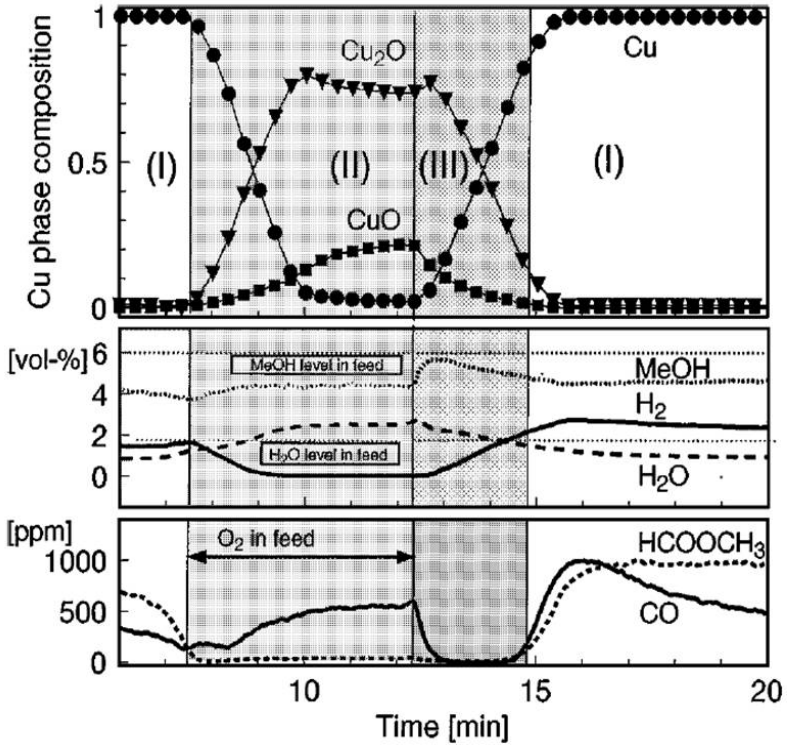

Fig. 8: Evolution of Cu phase composition of a Cu/ZnO catalyst during oxygen addition cycles into steam reforming feed at 523 K. Phase analysis was based on the corresponding X-ray absorption near edge structure (XANES) spectra. The two lower sections of the graph depict the evolution of the gas-phase in percent and ppm, respectively. Three transitions in bulk and gas-phase composition are marked: (I) copper metal during steam reforming, (II) oxidation to of Cu, (III) and re-reduction of Cu oxide. Reprinted from ref [120] with permission from Elsevier.

Accordingly, short addition of oxygen to a Cu/ZrO_2 MSR catalyst under working conditions was also shown to have an activating ef-

fect on the Cu phase, which is even more pronounced and stable compared to Cu/ZnO [19,107]. In this case no significant lattice strain of Cu could be detected, but incorporation of oxygen in metallic Cu was observed (see above). Considering similar effects on the catalytic properties of Cu in these particular experiments but apparently different structural origins in Cu/ZnO and Cu/ZrO_2, and taking into account the work addressing the oxidation state of Cu, a general view on Cu in MSR emerges. The catalytic activity of Cu in MSR seems to be related to a non-equilibrium form of metallic Cu. The deviation of the catalytically active surface from its ordered equilibrium form can be triggered by redox-chemistry as well as by a beneficial microstructural arrangement of the composite catalyst. The former relates to a distortion of the Cu lattice by oxygen dissolution and is a dynamic effect, which adjusts itself *in situ*. This effect can be measured by bulk methods as residual oxygen content in the Cu^0 phase and may well influence the Cu^0/Cu^+ ratio measured *ex situ* with surface sensitive techniques. The extent of this distortion is a function of the gas phase composition and the metal-oxide interactions. Oxygen incorporation is favored by increasing the oxidation power of the feed, e.g. by oxygen addition, and facilitated by strong (or synergetic) interactions of Cu and the oxide component like in Cu/ZrO_2. However, oxidation of Cu to a bulk oxide form (Cu_2O) by a too strongly oxidizing atmosphere as well as formation of a mixed oxide phase (e.g. inactive $CuAl_2O_4$) by too strong interactions of Cu with the oxide has to be avoided.

Deviation from equilibrium Cu due to static defects and lattice strain, on the other hand, can be introduced in the Cu particles by proper catalyst preparation aiming at kinetically trapping a distorted and defect-rich state of Cu. In a microstructure with small particles, many Cu^0-oxide interfaces like in the commercial Cu/ZnO/(Al_2O_3) catalyst beneficially affect the Cu phase. In addition to the beneficial role of Zn^{2+} on Cu dispersion (see above), the interface of Cu metal and ZnO seems to be well suited to pin this favorable defect structure of Cu^0.

Intermetallic Compounds in Methanol Steam Reforming

Besides the Cu-based systems, different other systems, mainly based on palladium or platinum, have been explored as catalysts for the steam reforming of methanol. The driving force was to detect materials with higher stability against sintering and higher selectivity, i.e. lower CO partial pressures in the product [136].

Interestingly, the formation of intermetallic compounds is frequently observed in these metal-oxide supported systems and is very often connected with a significant increase in selectivity to CO_2 [27]. An "intermetallic compound" is composed of two or more metallic elements and possesses a crystal structure which is different from the constituting elements and at least partly ordered [137,138]. "Compound" implies, that it is single-phase, which is not in contradiction to the often broad homogeneity ranges of intermetallic compounds.

In contrast, the more familiar term “alloy” corresponds to a mixture of metals, intermetallic compounds and/or non-metals, and can consist of more than one phase.

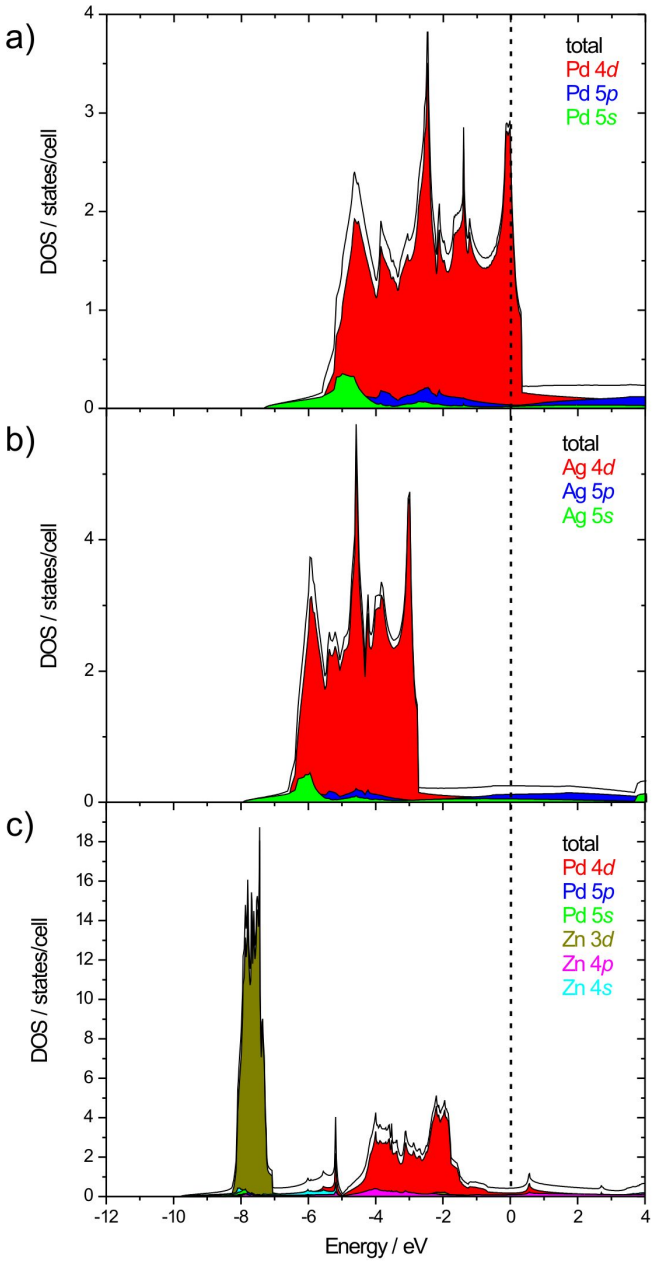

Figure 9: Density of states of metallic Pd (a), Ag (b) and the intermetallic compound ZnPd (c). Ag-Pd alloy formation leads to *d*-band filling intermediate between elemental Pd and Ag. In contrast, huge differences are revealed at the Fermi energy as well as in the width of the Pd *d*-bands upon formation of the intermetallic compound ZnPd (c).

Figure 9 demonstrates the huge consequences of an ordered intermetallic compound on the electronic structure of the catalytically active species. Opposed are the electronic densities of state (DOS) of Pd metal, Ag metal and the intermetallic compound ZnPd (often called PdZn but see [139]). By alloy-formation of e.g. Ag-Pd the total electron concentration per atom increases with increasing Ag-content, but the crystal structure does not change (Cu type of crystal structure, space group $Fm\bar{3}m$). As a consequence, the DOS remains very similar (so-called *rigid-band approach*) to that of elemental Pd but the *d*-bands are further populated until they reach the population of pure silver (Fig. 9b). On the other hand, the intermetallic compound ZnPd crystallizes in the ordered CuAu type of crystal structure (space group P4/*mmm*). The crystal structure is a direct consequence of the covalent chemical bonding within the intermetallic compound upon formation [139]. Interestingly, covalent interactions are quite common in intermetallic compounds, leading to a strong alteration of the electronic structure as seen in Fig. 9c. They are also displayed by the physical properties of the compounds [140-142]. Since a significant number of valence electrons are localized in the covalent bonds, the electrical conductivity is significantly reduced upon compound formation. An example is the well investigated θ-phase, the intermetallic compound $CuAl_2$ [142] in the system Al-Cu shown in Fig. 10.

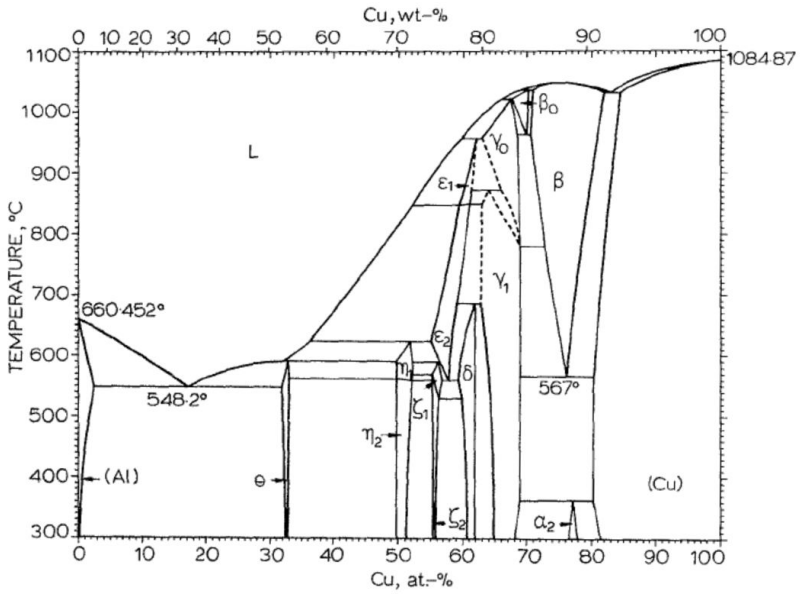

Fig. 10: Phase diagram of the system Al-Cu. Reprinted from Int. Met. Reviews 30, J.L. Murray, The aluminium-copper system, 211-233, with permission from ASM International®. All rights reserved. www.asminternational.org

Both elements crystallize in the Cu-type of structure (cubic closed packed). Alloy formation takes place on the Al- as well as the Cu-rich side. Up to 20 at.-% of Al can be dissolved in Cu without changing the crystal structure. Between the two alloys, a number of intermetallic compounds with different structures are formed. In $CuAl_2$ the three-bonded Al atoms build covalent and interpenetrating 6^3 nets. The Cu atoms are located in tetragonal antiprismatic cavities and interconnect the 6^3 nets by eight three-centre bonds. This bonding situation is dramatically influencing the physical properties. In contrast to Cu and Al, $CuAl_2$ is no longer ductile, but brittle as glass – a property often observed for covalently bonded intermetallic compounds. Localization of the electrons in the covalent bonds re-

duces the number of charge carriers and thus the electric resistivity is significantly increased to 7.6 μΩcm [143] at 295 K compared to $\rho_{295\ K,\ Cu}$ = 1.55 μΩcm and $\rho_{295\ K,\ Al}$ = 2.73 μΩcm. The strongly altered electronic and crystal structures determine the adsorption and the catalytic properties. Thus, it is necessary to keep the above mentioned differences between an intermetallic compound and an alloy in mind when looking at bi-metallic catalysts.

Staying with palladium, the direct consequences on the catalytic behavior upon compound formation can be demonstrated. While palladium possesses only a CO_2 selectivity of 0.9% in methanol steam reforming, formation of the intermetallic compound ZnPd leads to 98% CO_2 selectivity [144]. In the following, the different roles played by intermetallic compounds in the steam reforming of methanol are discussed. Starting with the deliberate decomposition of intermetallic compounds to synthesize highly active catalysts and via the observation of intermetallic compounds forming during time on stream this section ends with the use of well-defined intermetallic systems to systematically develop an understanding of the underlying principles of the steam reforming of methanol. The following sections do not aim at a complete review of the existing literature, but at revealing the different ideas concerning intermetallic compounds and the steam reforming of methanol present in literature.

Catalysts derived by decomposition of intermetallic compounds

Applying intermetallic compounds in methanol steam reforming is still a young scientific subject. The first appearance was in 1994 when Miyao et al. [145] used Al-Cu, Cu-Zn and Al-Cu-Zn alloys, which contained intermetallic compounds such as $CuAl_2$, CuZn and Cu_5Zn_8, as precursors to synthesize highly active Cu-based Raney-type catalysts. During leaching with aqueous NaOH, the intermetallic compounds are decomposed and the observed catalytic properties can not be correlated to the crystal and/or electronic structure of the starting materials. Typically the leaching results in supported Cu particles with high surface area and thus higher activities than conventional Cu-based systems.

Also single-phase intermetallic compounds like the well-investigated $CuAl_2$ [142] and even quasicrystalline phases, i.e. ordered but non-periodic intermetallic compounds, have been used as precursors for Raney-type catalysts (Fig. 11).

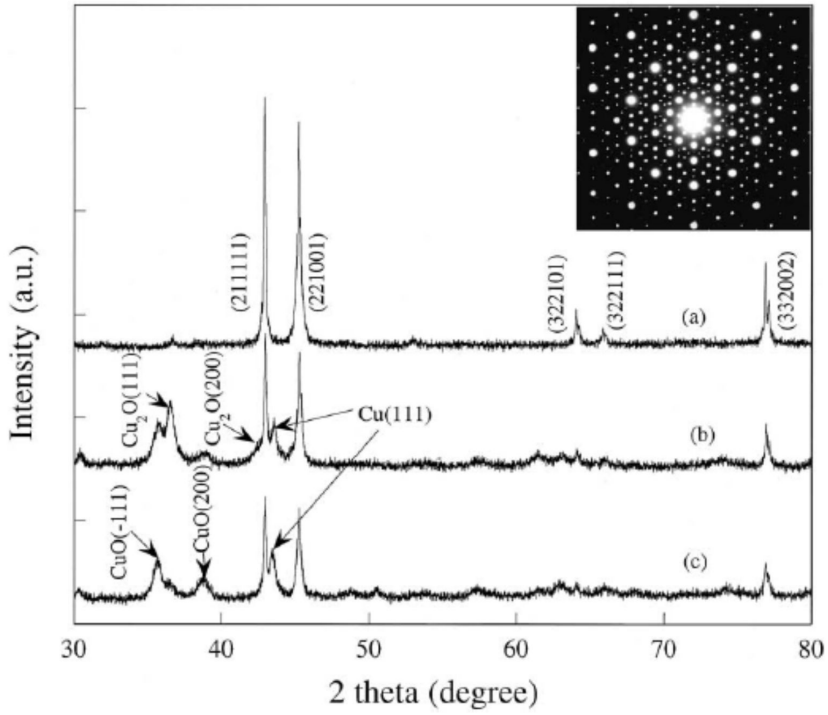

Figure 11: XRD of quasicrystalline $Al_{63}Cu_{25}Fe_{12}$ (a), after leaching with 20 wt.% NaOH at ambient temperature (b) and after use as methanol steam reforming catalyst (c). The inset shows an electron diffraction pattern of (a), proving the existence of the icosahedral quasicrystal. Reprinted from Appl. Catal. A 214, A.P. Tsai, T. Yoshimura, Highly active quasicrystalline Al-Cu-Fe catalyst for steam reforming of methanol, 237-241, Copyright 2001, with permission from Elsevier.

The group of Tsai leached powders of the quasicrystalline icosahedral i-Al-Cu-Fe phase, crystalline Al-Cu-Fe intermetallic compounds and $CuAl_2$ with NaOH or Na_2CO_3 [22,146-148]. This leads to a preferential dissolution of aluminum from the surface of the particles, leaving the intermetallic core untouched. The surface after leaching consists of transition metal particles which are dispersed on an aluminum hydroxide layer. As in the case of the abovementioned materials, the H_2 production rate increased to 235 L/kg, but the pres-

ence of iron also leads to a higher stability of the Cu particles against sintering. Interestingly, leaching of the quasicrystalline phase resulted in higher activity and stability compared to the crystalline intermetallic precursors – a phenomenon not understood yet. Ma et al. modified the leaching solution for $CuAl_2$ with Na_2CrO_4 and discovered that this increases the activity by a factor of two [23]. Using XPS, they could show, that the modification led to Cr_2O_3 promotion, which acts beneficial on the structural and catalytic properties. The presence of Cr_2O_3 results in higher BET surface areas due to higher porosity and smaller Cu particles. It was observed that Cr_2O_3 also increases the activity by itself, resulting in a higher activity compared to commercial copper chromite catalysts.

Another direction explored to generate high specific Cu surface areas is to oxidize intermetallic compounds or alloys prior to their use as catalysts. This approach is similar to a preparation of methanol synthesis catalysts which was developed in the 1970s by Wallace and Lambert [149,150]. Here the oxidation of Cu-*RE* (*RE* = rare earth element) intermetallic compounds like $CeCu_2$ or $NdCu_5$ in the CO/H_2 feed leads to finely dispersed Cu particles which are supported on the rare earth oxides (Fig. 12).

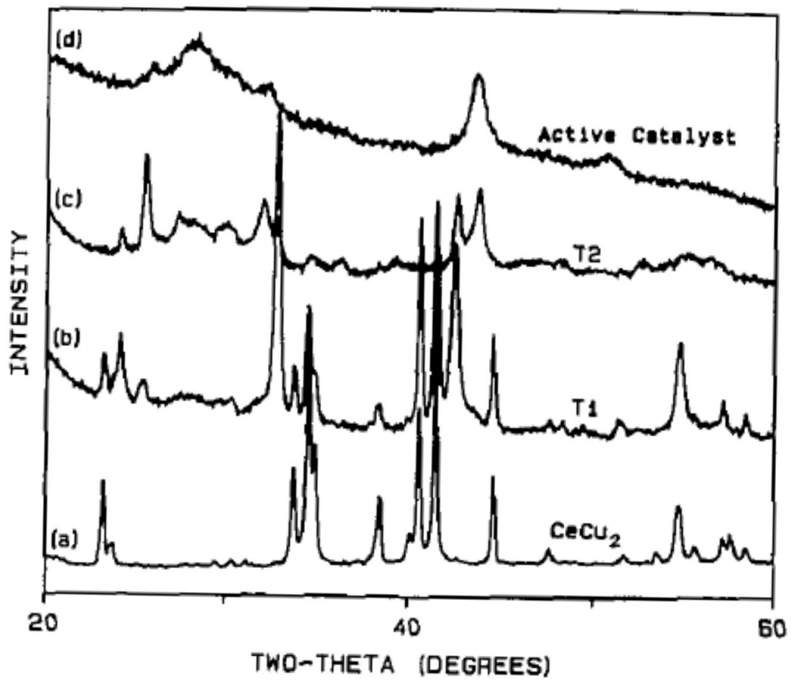

Figure 12: X-ray diffraction of $CeCu_2$ in He (a) and during treatment in 15 bar CO/H_2 at 353 K (b) and 373 K (c, d). The active state of the catalyst consists of Cu particles supported on CeO_2, while T1 and T2 show the decomposition of the intermetallic compound during the treatment. Reprinted from J. Catal. 106, R.M. Nix, T. Rayment, R.M. Lambert, J.R. Jennings, G. Owen, An in situ X-ray diffraction study of the activation and performance of methanol synthesis catalysts derived from rare earth-copper alloys, 216-234, Copyright 1987, with permission from Elsevier.

Activation of Ni_3Al in the methanol steam reforming feed leads to decomposition of the intermetallic compound to small Ni particles supported on oxidized/hydrolyzed aluminum [24]. While at a steam:carbon ratio of one both elements are oxidized, elemental Ni is preserved at a steam:carbon ratio of 0.1. The observed catalytic properties of the Ni_3Al-derived catalysts correspond to Ni-based catalysts and show CO_2-selectivities of only 10% since the main reaction – even under steam reforming conditions – is the decomposition of methanol.

To obtain high specific transition metal surface areas, Takahashi et al. oxidized amorphous Cu-Zr alloys with small contents of Au, Pd, Pt or Rh for 17 h in air at 570-587 K [25,151]. By subsequent reduction at 573 K in hydrogen, the desired supported transition metal catalysts were obtained. The most active catalysts were obtained from alloys with Pt and Rh contents around 1%, while for Au the activity increased with increasing Au content. The selectivity towards CO_2 of these catalysts was around 100% and it was concluded, that the main role of Pt, Rh and Au is to increase the copper dispersion. The behavior of the Pd modified Cu-Zr alloys differs significantly from the other alloys. While the activity is again increased, the selectivity to CO_2 is only around 60%. This can be attributed to the presence of elemental Pd which is an active catalyst for the decomposition of methanol to CO.

Besides being decomposed, intermetallic compounds are important in other ways in the steam reforming of methanol: On the one hand, they are often observed after the use of oxide supported catalysts, which triggered research on their formation. On the other hand, unsupported intermetallic compounds are under investigation to reveal their part in the steam reforming of methanol. Research on these two topics is compiled below.

Supported intermetallic compounds

As seen above, intermetallic compounds can be changed by the reactive atmosphere applied – but also conventional supported (monometallic) catalysts can be very dynamic systems. This is for example

expressed by deactivation due to sintering of the supported metal or the deposition of carbonaceous species.

Especially under reducing conditions (e.g. in the last step of the preparation) two other effects can be present. One is the so-called "strong metal-support interaction" (SMSI), which can be defined by three characteristics [152]: i) when reduced at low temperature, the catalyst shows a conventional chemical behavior, ii) high-temperature reduction strongly alters the chemisorption properties (SMSI state) and iii) the phenomenon is reversible by oxidation and mild reduction bringing the catalyst to state i). While in the first publication by Tauster the involvement of intermetallic compounds was suggested [153], the SMSI is today assigned to a covering of the metallic particles by a mobile and partly reduced support [155-156], a view that was also taken by Tauster in later publications [157]. The other phenomenon is the formation of intermetallic compounds by partial reduction of the (oxidic) support and subsequent reaction with the supported metal, for which we propose the term "reductive metal-support interaction" (RMSI). The formation of the intermetallic compounds has to be differentiated from the SMSI, since it is usually not reversible unless the catalysts are treated under very strong oxidizing conditions.

Instead of being formed before the reaction, intermetallic compounds can also be formed under reaction conditions by RMSI. Commonly, this process is not complete unless very high reduction temperatures are applied, where the necessary temperature depends on the combination of metal and support. Fig. 13 displays an exam-

ple of the problem. Using only XRD, it is hard to identify the species present after reduction at low temperatures. The observed diffraction patterns could be due to partially reduced PdO, solid solutions of oxygen or hydrogen in Pd or intermetallic compounds. If the process is not complete, different potentially catalytically active species can be present and the resulting complex systems (different metallic species, support, numerous interfaces …) hinder the determination of the catalytic properties of each of the components. While the RMSI is usually only observed in catalytic systems involving an easily reducible support (e.g. ZnO, Ge_2O_3, In_2O_3) – unless very high temperatures are applied [158,159] – the SMSI is not restricted to these systems and is also observed for ZrO_2 and Al_2O_3 [157].

Research for alternative methanol steam reforming catalysts providing higher stability than the Cu-based systems led to the investigation of Pd- and Pt-based catalysts. In the first publication by Iwasa et al. Pd and Pt on different supports were evaluated [160]. Normally, elemental Pd selectively catalyses the decomposition of methanol to CO, even in the presence of water, resulting in high CO contents in the product [161]. Surprisingly, Iwasa et al. observed that in the case of Pd/ZnO the CO_2 selectivity improved drastically from 0 to 97% with prior reduction of the catalyst.

By comparison of Pd/ZnO with Pd/SiO_2 and Pd/ZrO_2 they could show that by RMSI the intermetallic compound ZnPd is formed on Pd/ZnO, modifying strongly the catalytic selectivity of the Pd/ZnO catalyst [144]. On the other hand, no intermetallic compound was formed on Pd/SiO_2 or Pd/ZrO_2 at comparable temperatures, resulting

in low selectivities of 0.9% and 35% towards CO_2, respectively (Fig. 13).

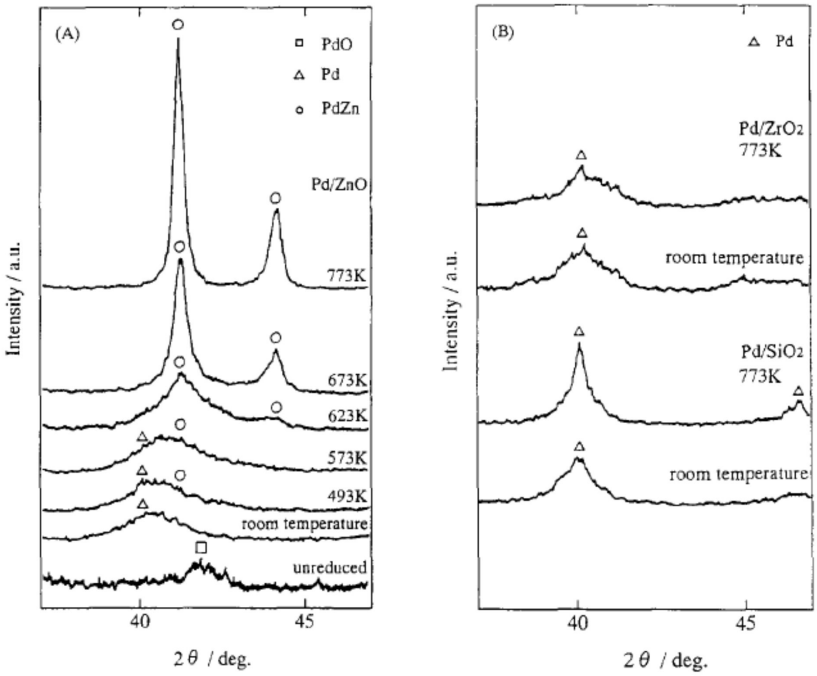

Figure 13: Powder X-ray diffraction of 10 wt.% Pd on ZnO (A), ZrO_2 and SiO_2 (B), respectively. The temperatures at which the catalysts were reduced are given in the figure. Reprinted from Appl. Catal. A 125, N. Iwasa, S. Masuda, N. Ogawa, N. Takezawa, Steam reforming of methanol over Pd/ZnO: Effect of the formation of PdZn alloys upon the reaction, 145-157, Copyright 1995, with permission from Elsevier.

In addition to XRD, the compound formation was also detected by X-ray photoelectron spectroscopy. The Pd $3d_{5/2}$ signal for elemental palladium is observed at 335.1 eV. The reductive treatment of Pd/ZnO at 673 K with hydrogen leads to a shift of 0.6 eV of the Pd $3d_{5/2}$ signal to higher binding energy.

The beneficial formation of ZnPd led to an increase of the conversion *and* selectivity from 33% and 62%, respectively, for Pd/ZnO catalysts reduced at 493 K to 58% and 98%, respectively, after re-

ductive treatment at 673 K. For comparison, the conversion over Pd/SiO_2 was 10% with a selectivity of 0.9% and Pd/ZrO_2 showed a conversion of 87% and a selectivity of 20%. It was suggested that the reason for the selectivity increase are the different reaction pathways for the decomposition of formaldehyde species on Pd and ZnPd. While they are selectively decomposed to CO and H_2 on elemental Pd, the intermetallic compound ZnPd leads to an effective attack by water and subsequent decomposition to CO_2 and H_2 similar to the reaction path suggested for Cu-based catalysts (Fig. 1).

These initial studies were followed by many others, making ZnPd/ZnO the best investigated intermetallic system for the steam reforming of methanol. Special interest lies on how the intermetallic particles are formed and how the catalytic properties depend on the particle size and morphology. The formation of the intermetallic compound has been investigated by two approaches so far. Wang et al. studied 15.9% Pd/ZnO prepared by co-precipitation by temperature programmed reduction, desorption, electric conductivity and XRD [162,163]. The strong interaction between metallic palladium and the support leads to hydrogen spillover during reduction. This enables the reduction of the ZnO in the vicinity of the Pd particles and the formation of the intermetallic compound ZnPd at temperatures above 523 K. The suggested reduction process follows the sequence $Pd/ZnO \rightarrow ZnPdO_{1-x}/ZnO \rightarrow ZnPd/ZnO$. For this catalyst, the best catalytic performance (41% conversion, 94% selectivity, hydrogen yield 0.65 $molg^{-1}h^{-1}$ at 523 K and a WHSV of 17.2 h^{-1})

was obtained after reduction at 573 K for 1 h in pure hydrogen, which resulted in a crystallite size of 5-14 nm.

A different approach was followed by Penner et al. [164], who synthesized well-defined thin film model systems by embedding epitaxially grown Pd-particles in an amorphous ZnO matrix which is mechanically stabilized by SiO_2. The advantage of this approach is the possibility to perform in depth TEM characterization on these materials. The formation of well-ordered ZnPd was observed at temperatures as low as 473 K and it was stable up to 873 K, where it partially decomposed into Pd-rich silicides. The epitaxial growth of the Pd particles causes their alike crystallographic orientation. This enabled the observation that the ZnPd intermetallic compound is formed by a topochemical reaction [165] starting at the surface of the Pd particles. Comparison of a similar Pd/SiO_2 thin film model revealed amorphisation of the Pd particles by reduction, most likely due to hydride formation. This clearly does not happen in the presence of ZnO as otherwise the crystallographic orientation between the particles would be lost. Most likely, hydrogen is activated on the Pd surface or a crystalline α-Pd-hydride with low hydrogen content is formed. A low concentration of activated hydrogen is reasonable because the hydrogen is used up by the reduction of the ZnO in the vicinity of the Pd-particles immediately. Thus, the most likely reaction sequence is Pd/ZnO → "PdH_x"/ZnO → ZnPd/ZnO, where "PdH_x" represents a crystalline Pd-hydride or activated hydrogen on the surface. Clarifying the intermediate in this reaction needs further investigation.

The influence of the ZnPd particle size (2 to 34 nm mean diameter) on the catalytic performance was studied by Dagle et al. and Karim et al. [166,167]. They found, that the intermetallic compound ZnPd is already formed at the relatively mild reduction temperature of 523 K. At these low temperatures, ZnPd and Pd co-exist on the support. By varying the reduction temperature, the Pd/ZnPd ratio was changed, but no monotonic correlation between ZnPd content and the CO_2 selectivity was observed. Instead, small particles showed CO_2 selectivities of only 62% compared to 99% for the larger ones and highly selective catalysts could be obtained by elimination of the small and unselective particles of the intermetallic compound. The loss in selectivity can be explained with a strong activity increase of small ZnPd particles in the reverse water-gas-shift reaction, thus, the production of CO by converting CO_2 and H_2 [168,169]. Interestingly, large ZnPd particles (diameter of 34 nm) show the same catalytic activity as small particles with 9 nm diameter. This might indicate that not only the intermetallic compound ZnPd, but also the ZnO support play important roles during catalysis, e.g. by forming the catalytically active interface together.

The influence of ZnO on the catalytic properties has been studied in more detail by using catalytic systems consisting of Pd and Zn being present on an inert support like carbon or alumina. Suwa et al. compared the deactivation behavior of ZnPd-ZnO/C and ZnPd/ZnO catalysts [170]. After 50 h time on stream, both catalysts showed deactivation from 70 to 60% and 70 to 40%, respectively. XRD analysis revealed the presence of $Zn_4CO_3(OH)_6*H_2O$ on the ZnPd/ZnO cata-

lyst. It was concluded that the deactivation mechanism is due to $Zn_4CO_3(OH)_6*H_2O$ covering the intermetallic surface. The stronger deactivation of ZnPd/ZnO compared to ZnPd-ZnO/C was explained by the higher amount on ZnO present on the former.

Another system on which the influence of ZnO has been studied is Pd-ZnO/Al_2O_3 [30]. A series of catalysts with different Pd loading and Pd:Zn molar ratios was prepared, characterized and tested. The highest selectivity (98.6%) and activity (80% conversion at 523 K) was revealed at a loading of 8.9% Pd with a Pd:Zn ratio of 0.38. Doubling the ratio led to a six times higher CO content, whereas with half the ratio the CO content reached 1.7%. By XRD, ZnO was observed at low Pd:Zn ratios, while at high Pd:Zn ratios elemental Pd was observed. This clearly shows, that an ideal Pd:Zn ratio exists. If not enough Zn is present, not all the Pd can be converted to ZnPd, thus catalytically decomposing the methanol to CO and H_2. Too high Zn contents on the other hand result in the formation of too much ZnO, which leads to lower selectivities and deactivation.

Pd/ZnO was also used in the oxidative steam reforming of methanol. Liu et al., who were the first to investigate this reaction/catalyst combination [171,172], studied in a series of publications the effect of the Pd-loading [173], the deactivation [174] and the influence of the presence of third metals [175]. In contrast to the steam reforming of methanol, the activity and selectivity increased with Pd loading, most probably due to the use of ZnO as support, thus not restricting the Pd:Zn ratio. Testing the catalysts over 25 h resulted in a deacti-

vation behavior superior to Cu-based catalysts, but with increasing amounts of CO (up to 18%) produced with time on stream (Fig. 14).

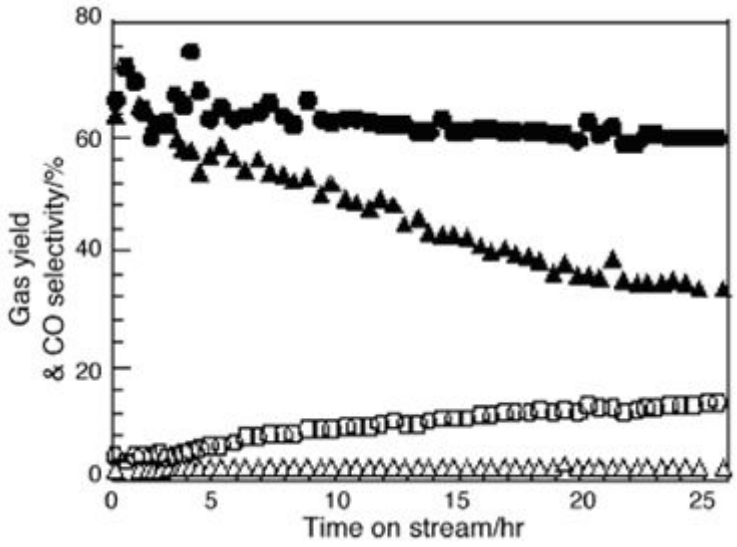

Fig. 14: Activity (solid symbols) and CO selectivity (open symbols) of Pd/ZnO (circles) and a commercial Cu/ZnO catalyst (triangles). Reprinted from Appl. Catal. A 299, S. Liu, K. Takajashi, K. Fuchigami, K. Uematsu, Hydrogen Production by Oxidative Methanol Reforming on Pd/ZnO: Catalyst Deactivation, 58-65, Copyright 2006, with permission from Elsevier.

By XPS investigations, it could be shown that the increasing CO content is due to a surface oxidation of the intermetallic compound ZnPd resulting in elemental palladium being present on the support, which leads to the decomposition of methanol. Modifying the Pd/ZnO co-precipitated catalysts with transition metals resulted in higher CO contents except in the cases of small amounts of Cr, Fe or Cu, which increased the selectivity slightly. The promotional effect was assigned to the water gas shift activity of these transition metals. The intrinsically lower selectivity of unpromoted Pd/ZnO/Al_2O_3 was

also observed for hydrotalcite derived catalysts, which showed CO_2 selectivities of 74-89% [176]. Thus it seems that using ZnPd in oxidative steam reforming is not a promising route to highly selective catalysts due to the decomposition of the selective intermetallic compound. In addition to methanol (oxidative) steam reforming, ZnPd has also been applied as catalyst for the partial oxidation of methanol [177-179] which is not in the focus of this chapter.

In summary, the catalytic system Pd/ZnO is quite complex. The different catalytic activities of ZnO, elemental Pd, ZnPd and the resulting interfaces pose a hurdle for a knowledge-based development and the empirical data base is not sufficient yet to draw final conclusions about the ongoing processes and the involved species. Large differences exist between different ZnPd/ZnO catalysts in the steam reforming of methanol (Table 1). These might be explained by different Pd:Zn ratios and varying ZnO contents as well as by particle size effects at two stages. Firstly, the catalytic properties change with particle size as shown above. Secondly, the formation of Pd-hydrides depends on the particle size [180-182] and if the formation of ZnPd is proceeding via a palladium hydride, size dependence during formation is expected. In consequence, each system and every preparation route involving ZnPd has its own ideal zinc content and reduction conditions which need to be explored and established.

Leaving the system Pd/ZnO and with it the intermetallic compound ZnPd, a number of other systems involving intermetallic compounds have been investigated for the steam reforming of methanol, albeit not yet in such depth as the aforementioned Pd/ZnO. Iwasa et al.

were the first to explore other transition metals supported on ZnO [27]. Amongst Ni, Co and Pt, only the latter formed an intermetallic compound (PtZn) during reduction. Compared to Pt/SiO_2 the CO_2 selectivity was enhanced from 25.6% to 95.6%. On the other hand, the Ni- and Co-based systems showed selectivities of 4.7 and 8.9%, respectively. Testing Pt-Zn/C, Ito et al. also observed a selectivity increase after formation of the intermetallic compound PtZn by reduction in H_2 at 873 K [183]. The resulting selectivity increase from 48% for Pt/C to 83% for PtZn/C was not as high as for PtZn/ZnO, probably indicating an uncompleted transformation of Pt.

In the next step, Iwasa et al. changed the support for the Pd- and Pt-based systems to Ga_2O_3 and In_2O_3 [26,28,184]. After reduction, the intermetallic compounds Pd_5Ga_2, $PdGa_5$, $Pd_{0.52}In_{0.48}$ (or PdIn), Pt_5Ga_3, $Pt_{10.6}Ga_{5.4}$ (or Pt_5Ga_3) and $PtIn_2$ were formed as observed by TPD, XRD, XPS and AES. Using Ga_2O_3 as support resulted in a mixture of intermetallic compounds in contrast to ZnO or In_2O_3 supported catalysts. As in the case of Pd/ZnO, the formation of the intermetallic compounds led to a large increase in the observed CO_2 selectivities. While the non-compound-forming systems Pd/SiO_2 and Pt/SiO_2 showed selectivities of 0 and 18.8%, respectively, the Ga-Pd and Ga-Pt intermetallic compounds raised the selectivity to 94.6 and 75.5%, respectively. In the case of the In_2O_3 supported catalysts, selectivities reached 95.5% for In-Pd intermetallic compounds and even 98.3% for In-Pt intermetallic compounds. Especially the latter nearly reaches that of ZnPd/ZnO catalysts, which possess a selectivity of 99.2% under the same conditions. $PdIn/Al_2O_3$ catalysts were

applied in a microstructured reactor [29]. According to this study, $PdIn/Al_2O_3$ seems to be a more dynamic system than ZnPd/ZnO. By undergoing a self-optimization by reduction in the feed and reaching a highly selective steady state, a pre-reduction is superfluous. To address the question why these intermetallic compounds behave so differently, the decomposition of formaldehyde, which is often claimed as intermediate in the steam reforming of methanol, was studied on elemental Pd and Pt catalysts as well as on the intermetallic compound catalysts. Here, a marked difference was observed: while the elements decomposed formaldehyde to CO, the intermetallic compounds selectively produced CO_2 [144,184]. This difference, as well as the different selectivities in the steam reforming of methanol, was assigned to the distinguished adsorption of the aldehyde in the η^1(O) structure on Cu, and the η^2(C,O) structure on Pd, Pt and Ni. It was proposed that the very different catalytic properties of ZnPd and metallic Pd are due to the different structures of the HCHO intermediates on the metals. However, this view is not corroborated by theoretical calculations, which propose very similar adsorption geometries for the HCHO intermediate on Cu and Pd (η^1) but η^2 for ZnPd [185]. The support portfolio was enlarged by GeO_2 (both the tetragonal and the hexagonal modification) and SnO_2 [186]. Pd supported on these supports forms under reducing conditions Pd_2Ge at 473 – 673 K and a mixture of Pd_2Sn and Pd_2Sn_3 at 573 K, respectively. In both cases, decomposition of methanol is the prevailing reaction, resulting in very low CO_2 selectivities in the steam reforming of methanol.

The formation of the Pd-based intermetallic compounds by reaction of the noble metal and the support was investigated – as in the case of ZnPd – in detail by thin film models by the group of Klötzer very recently. For these XRD, TEM and SEAD studies, small Pd particles were epitaxially grown on NaCl and this time covered with amorphous Ga_2O_3, In_2O_3, GeO_2 or SnO_2 [186,187]. To mimic the conditions of the synthesis of the catalysts used above, the Pd/Ga_2O_3 particles were first oxidized to PdO before being reduced at different temperatures in H_2. Reducing the particles at 523 K resulted first in Pd particles, which subsequently were transformed to the intermetallic compound Pd_5Ga_2 (Fig. 15).

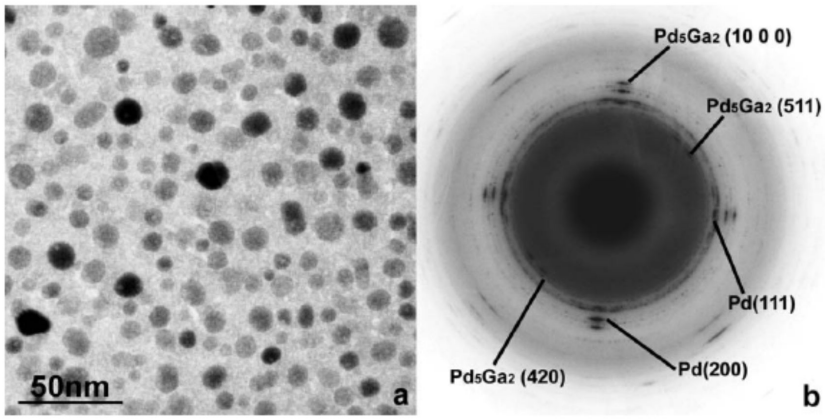

Figure 15: TEM image of Pd/Ga_2O_3 thin film catalyst after reduction in 1 bar H_2 (a). The corresponding SAED pattern is shown in (b). Reprinted from Appl. Catal. A 358, S. Penner, H. Lorenz, W. Jochum, M. Stöger-Pollach, D. Wang, C. Rameshan, B. Klötzer, Pd/Ga_2O_3 methanol steam reforming catalysts: Part I. Morphology, composition and structural aspects, 193-202, Copyright 2009, with permission from Elsevier.

The transformation is not complete, even when the reduction temperature is raised to 773 K. The remaining Pd is most probably located in the core of the particles, thus not taking part in the catalysis

directly. Above 673 K pronounced sintering of the particles was observed in contrast to ZnPd/ZnO. The study was complemented by investigating an impregnated Pd/β-Ga_2O_3 powder catalyst. In contrast to the thin film studies, the formation of the intermetallic compound Pd_2Ga [188] was observed here by XRD at reduction temperatures above 573 K. As in the thin films, elemental Pd is still present, even if the reduction is carried out at 773 K. Above 923 K, the Pd_2Ga is transformed to the intermetallic compound PdGa by further reduction of the support. In difference to the work of Iwasa, the intermetallic compound $PdGa_5$ was neither observed on the thin film nor on the powder catalyst after reduction.

In the case of the In_2O_3 supported catalyst also a thin film sample and a Pd/In_2O_3 powder catalyst were used to investigate the compound formation [189]. Two main differences to the former investigated systems occur in the Pd/In_2O_3 thin film samples: i) the deposited In_2O_3 is partly crystalline and not fully amorphous and ii) already during the deposition the formation of the intermetallic compound PdIn is observed. Reducing the thin film samples in H_2 at 373 K resulted in higher PdIn contents and at 573 K the In_2O_3 film is fully crystallized. From the TEM investigation of the PdIn particles, it was concluded, that the topochemical reaction growth follows the scheme PdIn[001]||Pd[001] and PdIn[011]||Pd[011]. At 573 K all the Pd is transformed to PdIn and the orientation of the particles is lost due to the stability limit of the In_2O_3 in hydrogen atmosphere. Reduction of the powder catalyst resulted in the complete transformation of Pd to PdIn at 573 K. As in the case of Ga_2O_3, higher tem-

peratures lead to the formation of the main group metal-richer intermetallic compounds Pd_2In_3 (673 K) and $PdIn_3$ (773 K).

Pd particles in a GeO_2 matrix are converted to Pd_2Ge at 473 to 573 K [186]. This transformation does not depend on the use of the GeO_2 modifications if the particles are conventionally supported and furthermore, the only intermetallic compound observed on the amorphous thin films is Pd_2Ge. In contrast, the intermetallic compounds observed for Pd on SnO_2 depend on whether a thin film sample with amorphous SnO_2 or a conventionally supported system is reduced at 573 K. In the first case, Pd_2Sn and Pd_3Sn_2 are observed, while in the thin films the reduction yields Pd_2Sn and PdSn. Kamiuchi et al. investigated the interaction between the Pd particles and the SnO_2 support [190]. After reduction at 673 K only the intermetallic compound Pd_3Sn_2 is formed and the particles are intruding into the support as revealed by subsequent TEM studies. During the short time of air-exposure, core-shell structures are formed by oxidation of the intermetallic tin on the surface. The core consists of the intermetallic compound Pd_3Sn_2 and the shell is an amorphous Sn-oxide corresponding to a SMSI state (see above). In contrast to the report by the group of Klötzer, Pd_2Sn was only observed after re-oxidation of the sample in air at 673 K in the non-SMSI state.

Despite the thorough investigation of the formation processes of the intermetallic compounds, it is a disadvantage of all aforementioned systems that the intermetallic compound is at least mixed with the support and in most cases also with the corresponding noble metal in the elemental state. Sometimes even more than one intermetallic

compound is present, bringing the complexity to an even higher level. In such systems, the number of possible catalytically active species hinders the assignment of the observed catalytic properties to a specific species and thus a knowledge-based development. The underlying processes might be complicated and most probably involve the support or the metal/support interfaces (at least in the case of ZnPd/ZnO, where this is indicated by the data available), but only reducing the complexity will allow to understand the role of the intermetallic compound. This approach can be followed either by theoretical calculations or by experiment and the progress achieved so far is summarized in the next section.

Unsupported intermetallic compounds

As seen in the large number of observations above, intermetallic compounds might play a pivotal role as catalysts for the steam reforming of methanol. However, the systems discussed so far do not allow an unambiguous correlation of the crystal and electronic structures of the intermetallic compounds and the observed catalytic properties for two reasons: i) the intermetallic compounds are not the only species present, and the support, e.g. ZnO, might also influence the catalytic properties; ii) the stability of the compounds needs to be proven under reaction conditions. While the impact of the first point is quite obvious, the second one can be exemplified by the subsurface carbon phase formation of palladium during the gas-phase hydrogenation of alkynes [191-193]. Here, the alkyne is decomposed on the surface and part of the the carbon forms a metastable

sub-surface Pd-C phase. The electronic structure of the material is changed significantly, which can be detected e.g. by XPS as a shift of the binding energy of the Pd $3d_{5/2}$ signal of 0.6 eV. As soon as the hydrocarbon supply is stopped, the subsurface Pd-C decomposes by segregation of the carbon to the surface. Before and after the reaction, only elemental palladium is observed (with carbon deposits after reaction), while the catalytically active phase actually is palladium modified by the sub-surface carbon. Changes like this need to be detected and studied to allow valid correlations. Modifications by hydrocarbons might not play a major role in the steam reforming of methanol. But some intermetallic compounds are known to readily form hydrides in hydrogen containing atmospheres. As in the case of carbon-modified palladium, this leads to a strong alteration of the electronic and sometimes the crystal structure, as has e.g. been studied in the case of $LaNi_5$ [194]. Besides hydride formation, decomposition of the intermetallic compounds can also occur as seen in the first section, demonstrating the need to prove the stability of the intermetallic compound in question under reaction conditions before correlating the electronic and crystal structure to the observed catalytic properties.

These requirements, i.e. to simplify the systems and prove their stability, can e.g. be fulfilled by performing experiments and quantum theoretical calculations on unsupported single-phase intermetallic compounds. Experimentally, this allows to detect changes to the materials much easier and, by proving the stability of the bulk and the surface, the resulting catalytic properties can be assigned directly to

the intermetallic compound and, thus, to its crystal and electronic structure. Quantum chemical calculations can provide information about the surface, like adsorption properties and possible reaction pathways. In addition, bulk quantum chemical calculations of the electron localizability function allow studying the chemical bonding in real space [195-196]. These calculations give valuable insight and help to understand the stability under reaction conditions.

To investigate the intrinsic catalytic properties and stabilities experimentally, three different kinds of materials can be used. The first is the unsupported intermetallic compound, usually prepared by metallurgical synthesis or in nanoparticulate form. Large single crystals represent the second class of materials and so called surface alloys the third. While the first is best suited in crushed form for reactor studies, the other two represent materials for surface science studies. Using unsupported intermetallic compounds as powders in a reactor and as single crystals in UHV studies allows to bridge the experimental “materials gap”. Ideally, the usually brittle single crystals can be comminuted after being studied in UHV and then be used for reactor studies. In addition, unsupported intermetallic compounds also allow closing the gap between quantum chemical calculations and experimental studies.

Nevertheless, there are material restrictions that one has to bear in mind. Surface alloys can be synthesized under UHV conditions by depositing e.g. Zn on a Pd single crystal and allow the Zn to react with the first few Pd layers. Complications arise, because the substrate and the surface alloy are usually electronic conducting materi-

als and the electronic structures influence each other. The surface alloy – even if it has the same crystal structure as the corresponding bulk-phase – thus possesses a modified electronic structure, which might result in altered adsorption and catalytic properties. Similar considerations are true for intermetallic compounds in nanoparticulate form. Here, size-confinement effects can alter the electronic structure compared to the bulk. Since the influence is not known unless one compares bulk and nanoparticulate samples, nanoparticulate intermetallic compounds are not suitable to determine the intrinsic catalytic properties.

As could be shown in the case of Pd-Ga intermetallic compounds in the semi-hydrogenation of acetylene [137,198-200], it is important to perform the experimental studies on well characterized and single-phase materials, which can be obtained best by metallurgical synthesis routes. In contrast to alloys, intermetallic compounds are often brittle and allow easy comminution after synthesis, e.g. by grinding or milling. Changes of the materials by these treatments need to be investigated in order to find the best suited route to generate higher active surface, while keeping the intrinsic structure.

The most studied intermetallic compound with respect to methanol steam reforming is ZnPd. These studies include the homogeneity range, chemical bonding and catalytic tests of the unsupported compound and extensive surface quantum chemical calculations. The range of existence of the tetragonal intermetallic compound ZnPd (CuAu type of structure, space group *P*4/*mmm*, a = 2.8931(1) Å and c = 3.3426(2) Å, c/a = 1.16) reaches from $Zn_{37.1(4)}Pd_{62.9(4)}$ to

$Zn_{50.9(1)}Pd_{49.1(1)}$ at 1173 K [139]. In contrast to the published binary phase diagram, the existence of the cubic high-temperature structure could not be confirmed experimentally in this reinvestigation. Quantum chemical tight-binding linear-muffin-tin-orbital (TB-LMTO) and full-potential local orbital (FPLO) calculations corroborated the experimental results and revealed a charge transfer from Zn to Pd of 0.4 e^-. Chemical bonding analysis by the electron localization indicator (ELI) revealed Pd-Pd interactions in the (001) plane as the driving force for the tetragonal distortion of ZnPd. The electronic density of states (DOS) around the Fermi energy of ZnPd is very similar to the DOS of elemental copper and led to the suggestion that both should possess similar catalytic performance (Fig. 16) [31,201,202].

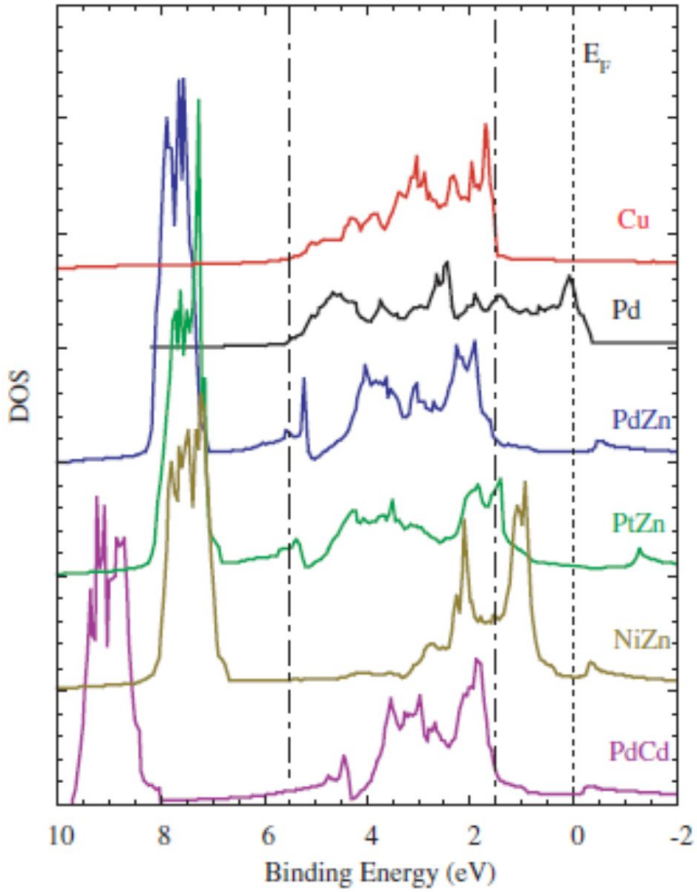

Figure 16: Electronic density of states for elemental Cu and Pd as well as for the intermetallic compounds ZnPd, PtZn, NiZn and PdCd. The dotted line represents the Fermi energy, while the two broken lines indicate the width of the Cu *d* states. Reprinted from J. Phys. Soc. Japan 73, A.P. Tsai, S. Kameoka, Y. Ishii, PdZn = Cu: Can an intermetallic compound replace an element?, 3270-3273, Copyright 2004, with permission from the Physical Society of Japan.

Further quantum chemical calculations show [203] that segregation is unlikely in accordance with the chemical bonding situation as described above. Out of the low-indexed surfaces, the (111) and (100) surface are calculated to be the most stable ones [201,204]. To elucidate the reaction mechanism, the group of Rösch performed surface quantum chemical calculations on ZnPd (111), (100) and

stepped (221) surfaces with Pd $(221)^{Pd}$ and Zn $(221)^{Zn}$, steps. Assuming the decomposition of methoxide (CH_3O) as being the rate limiting step in the steam reforming of methanol over Pd/ZnO, density functional calculations of the C-O and C-H bond breaking were performed. On all surfaces, the activation barrier of the C-H bond breaking is much lower than breaking the C-O bond, suggesting the first step in the decomposition is the abstraction of an H-atom. Nevertheless, calculations on defect-free ZnPd (111) and (100) surfaces revealed rather high activation barriers of 93 $kJmol^{-1}$ and 90 $kJmol^{-1}$ for the H-abstraction, respectively [205,206]. In contrast, the activation energy is lowered to around 50 $kJmol^{-1}$ in the case of the ZnPd $(221)^{Pd}$ surface [207]. The reason for the lower activation energy is twofold: i) the reactant CH_3O binds weaker to two Pd atoms of the step and ii) the resulting product CH_2O is bound stronger. For the abstraction of the H atom, two possible mechanisms have been identified. The first proceeds by tilting of the O-bound CH_3O towards the terrace followed by H-abstraction and possesses an activation energy of 49 $kJmol^{-1}$. In the second case, the C-O bond of the molecule is tilted towards the Pd-terminated step in the transition state and the H-atom is placed in an edge-bridge site, resulting in an activation barrier of 53 $kJmol^{-1}$. Due to the large differences in activation energy of flat and stepped surfaces, it was concluded that the reaction is catalyzed by steps or other defects on the surface. A factor not considered in the calculations so far is the presence of ZnO, which would result in a very complex system. Taking ZnO into account would be highly interesting, since the presence of ZnO could

have an influence on the catalytic properties according to the experimental studies on supported systems.

The earliest work on Pd-Zn surface alloys in UHV was performed on Pd-Zn/Ru(001) and Pd/Zn(0001) [208,209]. CO TDS on Pd-Zn/Ru(001) showed, that already very small amounts of Zn decrease the CO desorption energy dramatically. The full complexity of the Pd-Zn surface alloy(s) has been investigated and is still under investigation by several groups applying a broad range of methods using Zn/Pd(111) as common model system.

Deposition of Zn on Pd(111) below 300 K leads to elemental Zn multilayers, diffusion into the subsurface layers of Pd(111) starts at temperatures above 300 K. Temperatures of 400-500 K lead to a metastable buckled surface alloy of several layers with a p(2x1) LEED pattern (surface alloy 1 – SA1) [202,210,211]. Impact-collision ion scattering spectroscopy (ICISS) shows, that the Zn atoms are sticking out of the surface with a 1:1 composition [202,210,212]. At temperatures above 550 K, the Zn of the subsurface layers starts to diffuse into the bulk Pd, but the depletion is only slightly affecting the topmost layer [212]. At 623 K the diffusion of the Zn in subsurface layers has further progressed and a sub-surface Zn-diluted "monolayer" Pd-Zn surface alloy is obtained, which exhibits hardly any corrugation (SA2) [211-213]. The changes in the electronic structure by going from SA1 to SA2 are remarkable and result in a shift of the binding energy of the Pd3$d_{5/2}$ XPS signal of 335.3 to 335.6 eV and 335.9 eV for the 1 ML SA2 and a 3 ML SA1, respectively (Fig. 17).

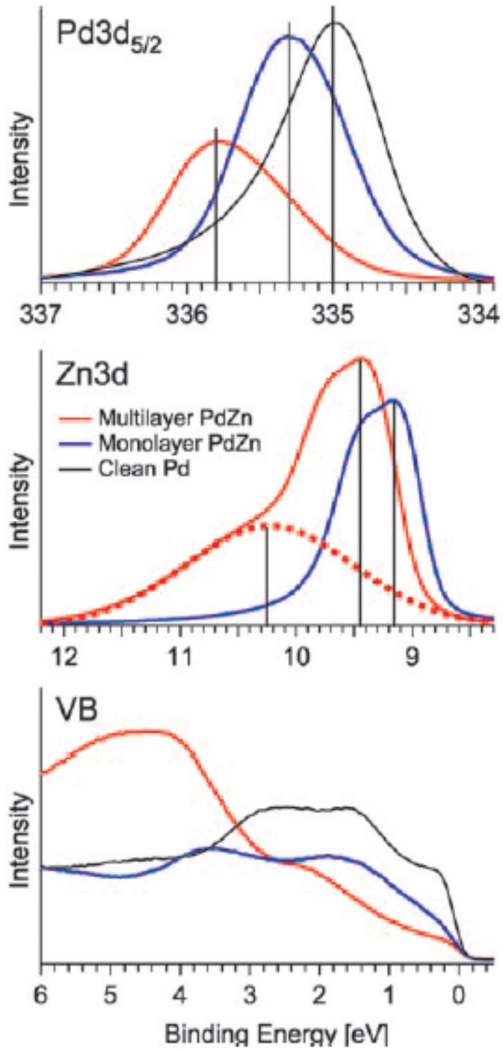

Figure 17: *In situ* X-ray photoelectron spectra (Pd 3*d*, Zn3*d* and valence band (VB) regions) showing the large electronic differences between elemental Pd (black, *ex situ*), the monolayer surface alloy SA2 (blue) and the multilayer surface alloy SA1 (red). The red dashed line in the middle panel corresponds to an oxidized ZnO(H) component formed during the *in situ* spectra acquisition. Reprinted from Angew. Chem. Int. Ed. 49, C. Rameshan, W. Stadlmayr, C. Weilach, S. Penner, H. Lorenz, M. Hävecker, R. Blume, T. Rocha, D. Teschner, A. Knop-Gericke, R. Schlögl, N. Memmel, D. Zemlyanov, G. Rupprechter, B. Klötzer, Subsurface-Controlled CO_2 Selectivity of PdZn Near-Surface Alloys in H_2 Generation by Methanol Steam Reforming, 3224-3227, Copyright 2010, with permission from Wiley-VCH Verlag GmbH & Co. KGaA.

If the deposition is performed at 300 K, ZnPd bilayer islands with a Pd:Zn ratio of 1:1 are formed, which are shown to be more stable than monolayer islands by DFT calculations [213,214]. In contrast to SA1 and SA2, a p(2x2) LEED pattern is reported if the layer is annealed at 520 K [215]. STM investigations revealed, that after deposition at 300 K three energetically identical p(2x1) domains are formed (SA3) explaining the p(2x2) LEED pattern [213,216]. As in the case of the multilayer alloy SA1 the surface of the bilayer islands of SA3 is not flat, but buckled with the Zn atoms sticking out [210,213]. If the whole surface is covered, additionally deposited Zn forms multilayers on top of SA3, which acts as a diffusion barrier at ambient temperature [213]. In difference to SA1, heating the Zn-covered sample to more than 600 K leads to partial Zn desorption and partial bulk diffusion of the additional Zn, before at 750 K the Zn of the SA3 starts to desorb [213]. As in the case of SA2, the buckling of the surface changes to Pd sticking out, as soon as the islands are reduced to one layer in thickness [213]. If the Zn deposition is carried out at 550 K, the p(2x1) LEED pattern characteristic for SA1 and SA2 is observed directly [202,217]. This indicates that at this temperature the ordered domains are much larger than after deposition at 300 K [217]. More complex surface structures have been observed after deposition of > 3 ML Zn at 750 K. This procedure leads to a well ordered ZnPd surface alloy with a (6x4√3/3) rectangular LEED pattern (SA4) corresponding to an 8-fold superstructure compared to the bulk structure [215].

The fcc structure of elemental Pd and the CuAu type of structure of ZnPd are closely related. Replacing Pd with Zn in an ordered manner would result in a *c*/*a* ratio of bulk ZnPd of 1.41. The experimentally determined ratio of 1.16 is significantly smaller, caused by the covalent bonding [137]. A bulk terminated (101) surface of ZnPd – corresponding to the Pd(111) surface – would result in a pseudo p(2x1) LEED pattern with $a' = 5.2833$ Å and $b' = 2.6416$ Å instead of the ideal values of $a = 5.4872$ Å and $b = 2.7436$ Å. Additionally, γ' would be 66.4° instead of the ideal 60.0° and the surface would be flat. However, no such deviations have been reported for the SA1 to SA4 yet. Since a comparison to the surface of bulk ZnPd is not possible yet, due to the challenges of growing such a crystal (> 1673 K are needed [218], which makes Zn very corrosive), the questions whether the underlying Pd(111) structure is causing a regular arrangement and the buckling, e.g. by modifying the electronic structure, can not be settled yet. The availability of a large ZnPd single crystal would also enable to settle the question how representative the results obtained for Zn/Pd(111) are for other intermetallic surfaces, which are definitively present in supported ZnPd/ZnO catalysts and in polycrystalline unsupported material.

What becomes clear by CO desorption measurements is the strong alteration of the chemical properties of the surface by Zn deposition and surface alloy formation. The desorption-maximum temperature is decreased by 220 K for SA1 and SA4 compared to a clean Pd(111) surface [217,218]. HREELS showed, that the decrease in desorption goes hand in hand with a change of CO being adsorbed in

three-fold hollow and bridged sites to adsorption on-top for the surface alloy [217]. This has direct influences for the steam reforming of methanol, since not only the adsorption of CO is altered, but also the activity of methanol dehydrogenation is strongly decreased [216]. The dehydrogenation activity starts to decrease at as low Zn contents as 0.03 ML and is nearly absent at coverages above 0.5 ML [216]. This behavior has been assigned to the changes of the preferred adsorption sites for the intermediates CH_3O and CH_2O [216]. The former adsorbs on 3-fold hollow sites involving one or two Zn atoms, while the latter adsorbs in a bridging mode on a Pd-Zn dimer in such a way, that the C atom is bonded to the Pd and the O is bonded to the Zn atom.

Even more striking is the different catalytic behavior of SA1 and SA2 in the steam reforming of methanol, which has recently been investigated [211]. With the electronic structure, also the catalytic properties in the steam reforming of methanol change dramatically (Fig. 17). While the thin surface alloy SA2 shows only very low selectivity towards CO_2 in the steam reforming of methanol, the multilayer surface alloy SA1 shows the expected high CO_2 selectivity. A thickness of SA1 of as little as five layers is sufficient to induce these strong changes of the catalytic properties. However, until the real structure of the working supported or bulk intermetallic catalyst is revealed, UHV studies on the clean surface-alloy material are helpful for comparison to e.g. Pd, but the catalytically active supported or bulk material might be much more complex.

Experimental catalytic studies on the bulk intermetallic compound ZnPd are very limited. Iwasa et al. synthesized Pd-Zn samples by heat treatment of physical mixtures of Pd and Zn at 220 to 673 K [219]. The resulting materials were investigated by XRD, which revealed the presence of Pd, Zn, ZnPd and/or $Zn_{6.1}Pd_{3.9}$ in the samples. Accordingly, the observed catalytic properties, e.g. the very low CO_2-selectivity of only 87.5%, can not be assigned to the intermetallic compound ZnPd. Metallurgic single-phase samples of ZnPd, PtZn, PdCd and NiZn were investigated by Tsai et al. [31]. The selection of the compounds was based on two considerations: i) they are all isostructural and ii) possess electronic structures which differ from ZnPd in the order PdCd < PtZn < NiZn. Fulfilling these criteria, the compounds allow investigating the electronic influence on the catalytic properties, since the geometric parameters are very similar by going from one compound to the other. The observed selectivities correspond to the expectations from the similarity of the electronic structures. At 553 K ZnPd and PdCd show selectivities close to 100%, PtZn possesses a CO_2 selectivity of 45% and NiZn only 10%. From these results, a strong influence of the electronic structure could be derived, provided the compound is stable *in situ*.

The *in situ* stability of the unsupported intermetallic compounds NiZn, PtZn and ZnPd has been investigated recently by our group applying high-pressure X-ray photoelectron spectroscopy in reactive atmosphere. When the intermetallic compound ZnPd is heated in vacuum to 573 K and a 1:1 molar ratio MeOH:H_2O mixture is intro-

duced subsequently, no changes occur in the Zn 3*d* signal, as seen in the valence band spectra shown in Figure 18.

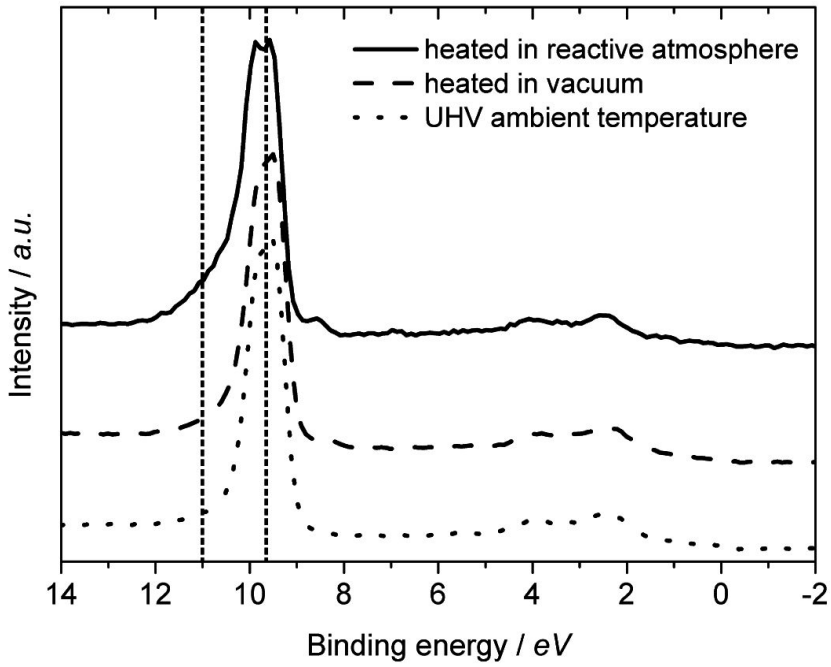

Figure 18: XPS valence band spectra of ZnPd: UHV conditions at ambient temperature (dotted line), *in situ* after heating to 573 K in UHV and subsequent switching to reactive atmosphere (0.2 mbar methanol/H_2O at a 1:1 ratio, dashed line) and *in situ* after heating to 573 K in reactive atmosphere (full line). Photon energy is set to 237 eV for all spectra.

On the other hand, heating ZnPd in MeOH/H_2O atmosphere from RT to 573 K leads to the development of a shoulder at 11 eV in the Zn 3*d* signal, proving the formation of an oxidized Zn species on the surface (Fig. 18). For PtZn, very similar results are obtained. Interestingly, the intermetallic compound ZnPd without the oxidized Zn species on the surface is catalytically less active in reactor tests by a factor of more than 35 compared to the intermetallic compound heated in reactive atmosphere. These results show for the first time

unambiguously, that ZnPd is not the only component of the active sites and that the oxidized Zn species plays a crucial role. On the other hand, too much ZnO is detrimental for the catalytic performance as proven by studies on supported catalysts.

The intermetallic compound NiZn undergoes severe surface changes under reaction conditions. The untreated surface in UHV consists of intermetallic Ni and Zn, as well as oxidized Zn species as detected in the Zn 3*d* region. As soon as the reactive gases are introduced to the XPS chamber (0.2 mbar methanol/H_2O, 1:1 molar ratio, 573 K), the surface of the compound changes dramatically (Fig. 19).

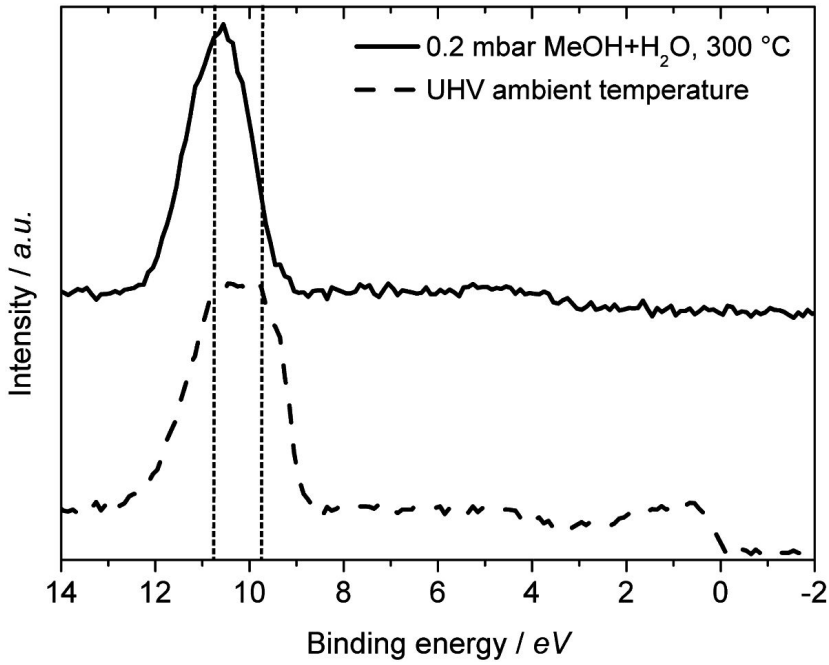

Figure 19: UHV (dashed) and *in situ* (full line) XPS valence band spectra of the intermetallic compound NiZn. Under UHV conditions, the metallic character is clearly seen at the Fermi energy. In reactive atmosphere, the Zn is completely oxidized and the density of states at the Fermi level is lost, indicating an oxidic overlayer. The incident photon energy is 301 eV for both spectra.

The intermetallic Zn on the surface is completely oxidized accompanied by a complete loss of the Ni core level signals in the most surface sensitive measurements. Thus, the methanol/H_2O mixture leads to segregation to and complete oxidation of the intermetallic Zn on the surface, forming a non-metallic and Ni-free surface layer on the surface of the compound. In the case of the intermetallic compound NiZn, the observed catalytic properties can not be attributed to the compound itself, but to the generated decomposition products.

The results of these investigations show, that the intermetallic surface of these three compounds is altered under reaction conditions. It would also have been very hard to detect the changes on a supported catalyst due to the presence of large amounts of ZnO, disguising the newly formed oxidized Zn species. The investigations demonstrate the advantage of using unsupported intermetallic compounds to study the role they (or their decomposition products) play in methanol steam reforming. These results also show that when investigating unsupported intermetallic compounds as catalysts, attention has to be paid to two issues: a) analysis is simpler on single phase samples and b) the *in situ* stability should be confirmed. Otherwise the identification of the intrinsic catalytic properties is hindered.

Robert Schlögl is greatly acknowledged for fruitful discussions and support. MB thanks the members of the Inorganic Chemistry Department of the Fritz Haber Institute for their help, support and discussions. MA thanks M. Friedrich for performing quantum chemical calculations and the Helmholtz Zentrum Berlin for providing BESSY beamtime 2009_1_80693 and continuing support during the XPS measurements. Networking within COST Action CM0904 “Network for Intermetallic Compounds as Catalysts in the Steam Reforming of Methanol” nurtured this publication.

References

[1] Sato M (1998) R&D activities in Japan on methanol synthesis from CO_2 and H_2. Catal. Surv. Jap. 2:175-184.

[2] Olah GA, Goeppert A, Surya Prakash GK (2006) Beyond Oil and Gas: The Methanol Economy. Wiley-VCH, Weinheim.

[3] Schlögl R (2010) The Role of Chemistry in the Energy Challenge. Chem. Sus. Chem. 3:209-222.

[4] Christiansen JA (1921) A reaction between methyl alcohol and water and some related reactions. J. Am. Chem. Soc. 43:1670-1672.

[5] Prigent M (1997) On board hydrogen generation for fuel cell powered electric cars - A review of various available techniques. Rev. Inst. Franc. Pét. 52:349-359.

[6] Navarro RM, Peña MA, Fierro JLG (2007) Hydrogen production reactions from carbon feedstocks: Fossils fuels and biomass. Chem. Rev. 107:3952-3991.

[7] Sá S, Silva H, Brandão L, Sousa JM, Mendes A (2010) Catalysts for methanol steam reforming-A review. Appl. Catal. B 99:43-57.

[8] De Wild PJ, Verhaak MJFM (2000) Catalytic production of hydrogen from methanol. Catal. Today 60:3-10.

[9] Joensen F, Rostrup-Nielsen JR (2002) Conversion of hydrocarbons and alcohols for fuel cells. J. Power Sources 105:195-201.

[10] Cheekatamarla PK, Finnerty CM (2006) Reforming catalysts for hydrogen generation in fuel cell applications. J. Power Sources 160:490-499.

[11] Palo DR, Dagle RA, Holladay JD (2007) Methanol steam reforming for hydrogen production. Chem. Rev. 107:3992-4021.

[12] Velu S, Suzuki K, Osaki T (1999) Oxidative steam reforming of methanol over CuZnAl(Zr)-oxide catalysts; a new and efficient method for the production of CO-free hydrogen for fuel cells. Chem. Commun. 2341–2342.

[13] Lattner JR, Harold MP (2007) Autothermal reforming of methanol: Experiments and modeling. Catal. Today 130:78-89.

[14] Park ED, Lee D, Lee HC (2009) Recent progress in selective CO removal in a H-2-rich stream. Catal. Today 139:280-290.

[15] Agrell J, Birgersson H, Boutonnet M, Melián-Cabrera I, Navarro RM, Fierro JLG (2003) Production of hydrogen from methanol over Cu/ZnO catalysts promoted by ZrO_2 and Al_2O_3 J. Catal. 219:389-403.

[16] Turco M, Bagnasco G, Costantino U, Marmottini F, Montanari T, Ramis G, Busca G (2004) Production of hydrogen from oxidative steam reforming of methanol - II. Catalytic activity and reaction mechanism on $Cu/ZnO/Al_2O_3$ hydrotalcite-derived catalysts. J. Catal. 228:56-65.

[17] Kurr P, Kasatkin I, Girgsdies F, Trunschke A, Schlögl R, Ressler T (2008) Microstructural characterization of $Cu/ZnO/Al_2O_3$ catalysts for methanol steam reforming - A comparative study. Appl. Catal. A 348:153-164.

[18] Velu S, Suzuki K (2003) Selective production of hydrogen for fuel cells via oxidative steam reforming of methanol over CuZnAl oxide catalysts: effect of substitution of zirconium and cerium on the catalytic performance. Topics in Catal. 22:235-244.

[19] Purnama H, Girgsdies F, Ressler T, Schattka JH, Caruso RA, Schomäcker R, Schlögl R (2004) Activity and selectivity of a nanostructured CuO/ZrO_2 catalyst in the steam reforming of methanol. Catal. Lett. 94:61-68.

[20] Ritzkopf I, Vukojevic S, Weidenthaler C, Grunwaldt JD, Schüth F (2006) Decreased CO production in methanol steam reforming over Cu/ZrO_2 catalysts prepared by the microemulsion technique. Appl. Catal. A 302:215-223.

[21] Liu Y, Hayakawa T, Suzuki K, Hamakawa S, Tsunody T, Ishii T, Kumagai M (2002) Highly active copper/ceria catalysts for steam reforming of methanol. Appl. Catal. A 223:137-145.
[22] Tsai AP, Yoshimura M (2001) Highly Active Quasicrystalline Al-Cu-Fe Catalyst for Steam Reforming of Methanol. Appl. Catal. A 214:237-241.
[23] Ma L, Gong B, Tran T, Wainwright MS (2000) Cr_2O_3 Promoted Skeletal Cu Catalysts for the Reactions of Methanol Steam Reforming and Water Gas Shift. Catal. Today 63:499-505.
[24] Jang JH, Xu Y, Chun DH, Demura M, Wee DM, Hirano T (2009) Effects of Steam Addition on the Spontaneous Activation in Ni_3Al Foil Catalysts during Methanol Decomposition. J. Molec. Catal. A 307:21-28.
[25] Takahashi T, Inoue M, Kai T (2001) Effect of Metal Composition on Hydrogen Selectivity in Steam Reforming of Methanol over Catalysts Prepared from Amorphous Alloys. Appl. Catal. A 218:189-195.
[26] Iwasa N, Nomura W, Mayanagi T, Fujita SI, Arai M, Takezawa N (2004) Hydrogen Production by Steam Reforming of Methanol. J. Chem. Engin. Japan 37:286-293.
[27] Iwasa N, Masuda S, Takezawa, N (1995) Steam Reforming of Methanol over Ni, Co, Pd and Pt Supported on ZnO. React. Kinet. Catal. Lett. 55:349-353.
[28] Iwasa N, Mayanagi T, Ogawa N, Sakata K, Takezawa N (1998) New Catalytic Functions of Pd-Zn, Pd-Ga, Pd-In, Pt-Zn, Pt-Ga and Pt-In Alloys in the Conversion of Methanol. Catal. Lett. 54:119-123.
[29] Iwasa N, Nomura W, Mayanagi T, Fujita SI, Arai M, Takezawa N (2004) Hydrogen Production by Steam Reforming of Methanol. J. Chem. Engin. Japan 37:286-293.
[30] Xia G, Holladay JD, Dagle RA, Jones EO, Wang Y (2005) Development of Highly Active Pd-ZnO/Al_2O_3 Catalysts for Microscale Fuel Processor Applications. Chem. Engin. Technol. 28:515-519.
[31] Tsai AP, Kameoka S, Ishii Y (2004) PdZn = Cu: Can an Intermetallic Compound Replace an Element? J. Phys. Soc. Japan 73:3270-3273.
[32] Jiang CJ, Trimm DL, Wainwright MS, Cant NW (1993) Kinetic Mechanism for the Reaction Between Methanol and Water over A Cu-ZnO-Al_2O_3 Catalyst. Appl. Catal. A 97:145-158.
[33] Takezawa N, Iwasa N (1997) Steam reforming and dehydrogenation of methanol: Difference in the catalytic functions of copper and group VIII metals. Catal. Today 36:45-56.
[34] Peppley BA, Amphlett JC, Kearns LM, Mann RF (1999) Methanol-steam reforming on Cu/ZnO/Al_2O_3 catalysts. Part 2. A comprehensive kinetic model. Appl. Catal. A 179:31-49.
[35] Rozovskii AY, Lin GI (2003) Fundamentals of methanol synthesis and decomposition. Top. Catal. 22:137-150.
[36] Lee JK, Ko JB, Kim DH (2004) Methanol steam reforming over Cu/ZnO/Al_2O_3 catalyst: kinetics and effectiveness factor. Appl. Catal. A 278:25-35.
[37] Peppley BA, Amphlett JC, Kearns LM, Mann RF (2005) Methanol–steam reforming on Cu/ZnO/Al2O3. Part 1: the reaction network. Appl. Catal. A 179:21-29.
[38] Frank B, Jentoft FC, Soerijanto H, Kröhnert J, Schlögl R, Schomäcker R (2007) Steam reforming of methanol over copper-containing catalysts: Influence of support material on microkinetics. J. Catal. 246:177-192.
[39] Kasatkin I, Kurr P, Kniep B, Trunschke A, Schlögl R (2007) Role of Lattice Strain and Defects in Copper Particles on the Activity of Cu/ZnO/Al_2O_3 Catalysts for Methanol SynthesisAngew. Chem. 119:7465-7468.
[40] Chinchen GC, Hay CM, Vanderwell HD, Waugh KC (1987) The measurement of copper surface areas by reactive frontal chromatography. J. Catal. 103:79-86.
[41] Hinrichsen O, Genger T, Muhler M (2000) Chemisorption of N_2O and H-2 for the surface determination of copper catalysts. Chem. Eng. Technol. 11:956-959.

[42] Naumann d'Alnoncourt R, Graf B, Xia X, Muhler M (2008) The back-titration of chemisorbed atomic oxygen on copper by carbon monoxide investigated by microcalorimetry and transient kinetics. J. Therm. Anal. Calor. 91:173-179.
[43] Behrens M, Furche A, Kasatkin I, Trunschke A, Busser W, Muhler M, Kniep B, Fischer R, Schlögl R (2010) The Potential of Microstructural Optimization in Metal/Oxide Catalysts: Higher Intrinsic Activity of Copper by Partial Embedding of Copper Nanoparticles. Chem. Cat. Chem. 2:816-818.
[44] Spencer MS (1999) The role of zinc oxide in Cu ZnO catalysts for methanol synthesis and the water-gas shift reaction. Top. Catal. 8:259-266.
[45] Hansen JB, Højlund Nielsen PE (2008) Methanol Synthesis. In: Ertl G, Knözinger H, Schüth F, Weitkamp J (eds) Handbook of Heterogenous Catalysis, 2nd edn. Wiley-VCH, Weinheim, 2920-2949.
[46] Naumann d'Alnoncourt R, Xia X, Strunk J, Löffler E, Hinrichsen O, Muhler M (2006) The influence of strongly reducing conditions on strong metal-support interactions in Cu/ZnO catalysts used for methanol synthesis. Phys. Chem. Chem. Phys. 13:1525-1538.
[47] Grunwaldt JD, Molenbroek AM, Topsoe NY, Topsoe H, Clausen BS (2000) In situ investigations of structural changes in Cu/ZnO catalysts. J. Catal. 194:452-460.
[48] Hansen PL, Wagner JB, Helveg S, Rostrup-Nielsen JR, Clausen BS, Topsoe H (2002) Atom-resolved imaging of dynamic shape changes in supported copper nanocrystals. Science 295:2053–2055.
[49] Spencer MS (1995) On the Activation-Energies of the Forward and Reverse Water-Gas Shift Reaction. Catal. Lett. 32:9-13.
[50] Twigg MV, Spencer MS (2003) Deactivation of copper metal catalysts for methanol decomposition, methanol steam reforming and methanol synthesis. Top. Catal. 22:191-203.
[51] Hughes R (1994) Deactivation of catalysts. Academic Press, New York.
[52] Kasatkin I et al., unpublished.
[53] Löffler DG, McDermott SD, Renn CN (2003) Activity and durability of water-gas shift catalysts used for the steam reforming of methanol. J. Power Sources 114:15-20.
[54] Thurgood CP, Amphlett JC, Mann RF, Peppley BA (2003) Deactivation of $Cu/ZnO/Al_2O_3$ catalyst: evolution of site concentrations with time. Topics Catal. 22:253-259.
[55] Agarwal V, Patel S, Pant KK (2005) H-2 production by steam reforming of methanol over Cu/ZnO/Al-2) catalysts: transient deactivation kinetics modeling. Appl. Catal. A 279:155-164.
[56] Agrell J, Birgersson H, Boutonnet M (2002) Steam reforming of methanol over a $Cu/ZnO/Al_2O_3$ catalyst: a kinetic analysis and strategies for suppression of CO formation. J. Power Sources 106:249-257.
[57] Schimpf S, Muhler M (2009) Methanol Catalysts. In: Krijn de Jong (eds) Synthesis of Solid Catalysts. Wiley-VCH, Weinheim, 329-351.
[58] Bems B, Schur M, Dassenoy A, Junkes H, Herein D, Schlögl R (2003) Relations between synthesis and microstructural properties of copper/zinc hydroxycarbonates. Chem. Eur. J. 9:2039-2052.
[59] Baltes C, Vukojevic S, Schüth F (2008) Correlations between synthesis, precursor, and catalyst structure and activity of a large set of $CuO/ZnO/Al_2O_3$ catalysts for methanol synthesis. J. Catal. 258:334-344.
[60] Shen GC, Fujita SI, Takezawa N (1992) Preparation of Precursors for the Cu/ZnO Methanol Synthesis Catalysis by Coprecipitation Methods - Effects of The Preparation Conditions upon the Structures of the Precursors. J. Catal. 138:754-758.
[61] Günter MM, Ressler T, Bems B, Büscher C, Genger T, Hinrichsen O, Muhler M, Schlögl R (2001) Implication of the microstructure of binary Cu/ZnO catalysts for their catalytic activity in methanol synthesis. Catal. Lett. 71:37-44.
[62] Waller D, Stirling D, Stone FS, Spencer MS (1989) Copper-Zinc Oxide Catalysts - Activity in Relation to Precursor Structure and Morphology. Faraday Dissuss. Chem. Soc. 87:107-120.

[63] Li JL, Inui T (1996) Characterization of precursors of methanol synthesis catalysts, copper zinc aluminum oxides, precipitated at different pHs and temperatures. Appl. Cat. A 137:105-117.
[64] Whittle DM, Mirzaei AA, Hargreaves JSJ, Joyner RW, Kiely CJ, Taylor SH, Hutchings GJ (2002) Co-precipitated copper zinc oxide catalysts for ambient temperature carbon monoxide oxidation: effect of precipitate ageing on catalyst activity. Phys. Chem. Chem. Phys. 4:5915-5920.
[65] Kniep BL, Ressler T, Rabis A, Girgsdies F, Baenitz M, Steglich F, Schlögl R (2003) Ratioal Design of Nanostructured Copper-Zinc Oxide Catalysts for the Steam Reforming of Methanol. Angew. Chem Intern. Ed. 43:112-115.
[66] Behrens M, Brennecke D, Girgsdies F, Kißner S, Trunschke A, Nasrudin N, Zakaria S, Fadilah Idris N, Bee Abd Hamid S, Kniep B, Fischer R, Busser W, Muhler M, Schlögl R (2011) Understanding the complexity of a catalyst synthesis: Co-precipitation of mixed Cu,Zn,Al hydroxycarbonate precursors for $Cu/ZnO/Al_2O_3$ catalysts investigated by titration experiments. Appl. Catal A 392:93-102.
[67] Behrens M (2009) Meso- and nano-structuring of industrial $Cu/ZnO/(Al_2O_3)$ catalysts J. Catal. 267:24-29.
[68] Schüth F, Hesse M, Unger KK (2008) Precipitation and Coprecipitation. In: Ertl G, Knözinger H, Schüth F, Weitkamp J (eds) Handbook of Heterogeneous Catalysis, 2nd edn. Wiley-VCH, Weinheim, 100-119.
[69] Lok M. (2009) Coprecipitation. In: Krijn de Jong (eds) Synthesis of Solid Catalysts. Wiley-VCH, Weinheim, 135-151.
[70] Kniep BL, Girgsdies F, Ressler T (2005) Effect of precipitate aging on the microstructural characteristics of Cu/ZnO catalysts for methanol steam reforming. J. Catal. 236:34-44.
[71] Millar GJ, Holm IH, Uwins PJR, Drennan J (1998) Characterization of precursors to methanol synthesis catalysts Cu/ZnO system. J. Chem. Soc. Faraday Trans. 94:593-600.
[72] Behrens M, Girgsdies F, Trunschke A, Schlögl R (2009) Minerals as Model Compounds for Cu/ZnO Catalyst Precursors: Structural and Thermal Properties and IR Spectra of Mineral and Synthetic (Zincian) Malachite, Rosasite and Aurichalcite and a Catalyst Precursor Mixture. Eur. J. Inorg. Chem. 10:1347-1357.
[73] Fujita S, Satriyo AM, Shen GC, Takezawa N (1995) Mechanism of the Formation of Precursors for the Cu/ZnO Methanol Synthesis Catalysts by a Coprecipitation Method. Catalysis Letters 34:85-92.
[74] Behrens M, Girgsdies F (2010) Structural Effects of Cu/Zn Substitution in the Malachite-Rosasite System. Z. Anorg. Allg. Chem. 636:919-927.
[75] Shen GC, Fujita S, Matsumoto S, Takezawa N (1997) Steam reforming of methanol on binary Cu/ZnO catalysts: Effects of preparation condition upon precursors, surface structure and catalytic activity. J. Mol. Catal. A 124:123-136.
[76] Shishido T, Yamamoto Y, Morioka H, Takaki K, Takehira K (2004) Active Cu/ZnO and $Cu/ZnO/Al_2O_3$ catalysts prepared by homogeneous precipitation method in steam reforming of methanol. Appl. Catal. A 263:249-253.
[77] Shishido T, Yamamoto Y, Morioka H, Takehira K (2007) Production of hydrogen from methanol over Cu/ZnO and $Cu/ZnO/Al_2O_3$ catalysts prepared by homogeneous precipitation: Steam reforming and oxidative steam reforming. J. Mol. Catal. A 268:185-194.
[78] Zhang XR, Wang LC, Yao CZ, Cao Y, Dai WL, He HY, Fan KN (2005) A highly efficient $Cu/ZnO/Al_2O_3$ catalyst via gel-coprecipitation of oxalate precursors for low-temperature steam reforming of methanol. Catal. Lett. 102:183-190.
[79] Wang LC, Liu YM, Chen M, Cao Y, He HY, Wu GS, Dai WL, Fan KN (2007) Production of hydrogen by steam reforming of methanol over Cu/ZnO catalysts prepared via a practical soft reactive grinding route based on dry oxalate-precursor synthesis. J. Catal. 246:193-204.
[80] Becker M, Naumann d'Alnoncourt R, Kähler K, Sekulic J, Fischer RA, Muhler M (2010) The Synthesis of Highly Loaded Cu/Al_2O_3 and $Cu/ZnO/Al_2O_3$ Catalysts by the Two-Step

CVD of Cu(II)diethylamino-2-propoxide in a Fluidized-Bed Reactor. Chem. Vap. Deposition 16:85-92.
[81] Kurtz M, Bauer N, Büscher C, Wilmer H, Hinrichsen O, Becker R, Rabe S, Merz K, Driess M, Fischer RA, Muhler M (2004) New synthetic routes to more active Cu/ZnO catalysts used for methanol synthesis. Catal. Lett. 92:49-52.
[82] Omata K, Hashimoto M, Wanatabe Y, Umegaki T, Wagatsuma S, Ishiguro G, Yamada M, (2004) Optimization of Cu oxide catalyst for methanol synthesis under high CO_2 partial pressure using combinatorial tools. Appl. Catal. A 262:207-214.
[83] Breen JP, Ross JRH (1999) Methanol reforming for fuel-cell applications: development of zirconia-containing Cu-Zn-Al catalysts. Catal. Today 51:521-533.
[84] Matsumura Y, Ishibe H (2009) Suppression of CO by-production in steam reforming of methanol by addition of zinc oxide to silica-supported copper catalyst. J. Catal. 268:282-289.
[85] Yang HM, Liao PH (2007) Preparation and activity of Cu/ZnO-CNTs nano-catalyst on steam reforming of methanol. Appl. Catal. A 317:226-233.
[86] Kudo S, Maki T, Miura K, Mae K (2010) High porous carbon with Cu/ZnO nanoparticles made by the pyrolysis of carbon material as a catalyst for steam reforming of methanol and dimethyl ether. Carbon 48:1186-1195.
[87] Cavani F, Trifirò F, Vaccari A (1991) Hydrotalcite-type anionic clays: Preparation, properties and applications. Catal. Today 11:173-301.
[88] Takehira K, Shishido T (2007) Preparation of supported metal catalysts starting from hydrotalcites as the precursors and their improvements by adopting "memory effect". Catal. Surv. Asia 11:1-30.
[89] Tang Y, Liu Y, Zhu P, Xue Q, Chen L, Lu Y (2009) High-performance HTLcs-derived CuZnAl catalysts for hydrogen production via methanol steam reforming. Am. Inst. Chem. Eng. J. 55:1217-1228.
[90] Busca G, Constatino U, Marmottini F, Montanari T, Patrono P, Pinari F, Ramis G (2006) Methanol steam reforming over ex-hydrotalcite Cu–Zn–Al catalysts. Appl. Catal. A 310:70-78.
[91] Behrens M, Kasatkin I, Kühl S, Weinberg G (2010) Phase-Pure Cu,Zn,Al Hydrotalcite-like Materials as Precursors for Copper rich $Cu/ZnO/Al_2O_3$ Catalysts. Chem. Mater. 22:386-397.
[92] Kühl S, Friedrich M, Armbrüster M, Behrens M, unpublished.
[93] Turco M, Bagnasco G, Costantino U, Marmottini F, Montanari T, Ramis G, Busca G (2004) Production of hydrogen from oxidative steam reforming of methanol - I. Preparation and characterization of $Cu/ZnO/Al_2O_3$ catalysts from a hydrotalcite-like LDH precursor. J. Catal. 228:43-55.
[94] Turco M, Bagnasco G, Cammarano C, Senese P, Costantino U, Sisani M (2007) $Cu/ZnO/Al_2O_3$ catalysts for oxidative steam reforming of methanol: The role of Cu and the dispersing oxide matrix. Appl .Catal. B 77:46-57.
[95] Velu S, Suzuki K, Okazaki M, Kapoor MP, Osaki T, Ohashi F (2000) Oxidative steam reforming of methanol over CuZnAl(Zr)-oxide catalysts for the selective production of hydrogen for fuel cells: Catalyst characterization and performance evaluation. J. Catal. 194:373-384.
[96] Velu S, Suzuki K, Kapoor MP, Ohashi F, Osaki T (2001) Selective production of hydrogen for fuel cells via oxidative steam reforming of methanol over CuZnAl(Zr)-oxide catalysts. Appl. Catal. A 213:47-63.
[97] Velu S, Suzuki K, Gopinath CS, Yoshida H, Hattori T (2002) XPS, XANES and EXAFS investigations of $CuO/ZnO/Al_2O_3/ZrO_2$ mixed oxide catalysts. Phys. Chem. Chem. Phys. 4:1990-1999.
[98] Breen JP, Ross JRH (1999) Methanol reforming for fuel-cell applications: development of zirconia-containing Cu-Zn-Al catalysts. Catal. Today 51:521-533.

[99] Matsumura Y, Ishibe H (2009) High temperature steam reforming of methanol over Cu/ZnO/ZrO_2 catalysts. Appl. Catal. B 91:524–532.
[100] Jones SD, Hagelin-Weaver HE (2009) Steam reforming of methanol over CeO_2- and ZrO_2-promoted Cu-ZnO catalysts supported on nanoparticle Al_2O_3. Appl. Catal. B 90:195–204.
[101] Idem RO, Bakhshi NN (1996) Characterization studies of calcined, promoted and non-promoted methanol-steam reforming catalysts. Can. J. Chem. Eng. 74:288-300.
[102] Lindström B, Pettersson LJ (2001) Hydrogen generation by steam reforming of methanol over copper-based catalysts for fuel cell applications. Int. J. Hydrogen Energy 26:923-933.
[103] Lindström B, Pettersson LJ, Menon PG (2002) Activity and characterization of Cu/Zn, Cu/Cr and Cu/Zr on gamma-alumina for methanol reforming for fuel cell vehicles. Appl. Catal. 234:111-125.
[104] Matsumura Y, Ishibe H (2009) Selective steam reforming of methanol over silica-supported copper catalyst prepared by sol-gel method. Appl. Catal. B 86:114-120.
[105] Kobayashi H, Takezawa N, Shimokawabe M, Takahashi K (1983) Preparation Of Copper Supported On Metal Oxides And Methanol Steam Reforming Reaction. Stud. Surf. Sci. Catal. 16:697-707.
[106] Takezawa N, Shimokawabe M, Hiramatsu H, Sugiura H, Asakawa T, Kobayashi H (1987) Steam Reforming of Methanol over Cu/ZrO_2 – Role of ZrO_2 Support. React. Kinet. Catal. Lett. 33:191-196.
[107] Szizybalski A, Girgsdies F, Rabis A, Wang Y, Niederberger M, Ressler T (2005) In situ investigations of structure-activity relationships of a Cu/ZrO_2 catalyst for the steam reforming of methanol. J. Catal. 233:297-307.
[108] Oguchi H, Kanai H, Utani K, Matsumura Y, Imamura S (2005) Cu_2O as active species in the steam reforming of methanol by CuO/ZrO_2 catalysts. Appl. Catal. A 293:64-70.
[109] Yao C, Wang L, Liu Y, Wu G, Cao Y, Dai W, He H, Fan K (2006) Effect of preparation method on the hydrogen production from methanol steam reforming over binary Cu/ZrO_2 catalysts. Appl. Catal. A 297:151-158.
[110] Wang LC, Liu Q, Chen M, Liu YM,. Cao Y, He HY, Fan KN (2007) Structural Evolution and Catalytic Properties of Nanostructured Cu/ZrO_2 Catalysts Prepared by Oxalate Gel-Coprecipitation Technique. J. Phys. Chem. C 111:16549-16557.
[111] Wu GS, Mao DS, Lu GZ, Cao Y, Fan KN (2009) The Role of the Promoters in Cu Based Catalysts for Methanol Steam Reforming. Catal. Lett. 130:177-184.
[112] Liu Y, Hayakawa T, Suzuki K, Hamakawa S (2001) Production of hydrogen by steam reforming of methanol over Cu/CeO_2 catalysts derived from $Ce_{1-x}Cu_xO_{2-x}$ precursors. Catal. Commun. 2:195-200.
[113] Liu Y, Hayakawa T, Tsunoda T, Suzuki K, Hamakawa S, Murato K, Shiozaki R, Ishii T, Kumagai M (2003) Steam reforming of methanol over Cu/CeO_2 catalysts studied in comparison with Cu/ZnO and Cu/Zn(Al)O catalysts. Top. Catal. 22:205-213.
[114] Mastalir A, Frank B, Szizybalski A, Soerijanto H, Deshpande A, Niederberger M, Schomäker R, Schlögl R, Ressler T (2005) Steam reforming of methanol over Cu/ZrO_2/CeO_2 catalysts: a kinetic study. J. Catal. 230:464-475.
[115] Oguchi H, Nishiguchi T, Matsumoto T, Kanai H, Utani K, Matsumura Y, Imamura S (2005) Steam reforming of methanol over Cu/CeO_2/ZrO_2 catalysts. Appl. Catal. A 281:69–73.
[116] Huang TJ, Chen HM (2010) Hydrogen production via steam reforming of methanol over Cu/(Ce,Gd)O_{2-x} catalysts. Int. .J. Hydrogen Energy 35:6218-6226.
[117] Bhagwat M, Ramaswamy AV, Tyagi AK, Ramaswamy V (2003) Rietveld refinement study of nanocrystalline copper doped zirconia. Mate. Res. Bull. 38:1713–1724.
[118] Fierro G, Lo Jacono M, Inversi M, Porta P, Cioci F, Lavecchia R (1996) Study of the reducibility of copper in CuO---ZnO catalysts by temperature-programmed reduction. Appl. Catal. A 137: 327-348.

[119] Noei H, Qiu H, Wang Y, Löffler E, Wöll C, Muhler M (2008) The identification of hydroxyl groups on ZnO nanoparticles by infrared spectroscopy. Phys. Chem. Chem. Phys. 10:7092-7097.
[120] Günther MM, Ressler T, Jentoft RE, Bems B (2001) Redox Behavior of Copper Oxide/Zinc Oxide Catalysts in the Steam Reforming of Methanol Studied by *in Situ* X-Ray Diffraction and Absorption Spectroscopy. J. Catal. 203:133-149.
[121] Goddby BE, Pemberton JE (1988) XPS Characterization of a Commercial $Cu/ZnO/Al_2O_3$ Catalyst: Effects of Oxidation, Reduction, and the Steam Reformation of Methanol. Appl. Spectros. 42:754-760.
[122] Raimondi F, Geissler K, Wambach J, Wokaun A (2002) Hydrogen production by methanol reforming: post-reaction characterisation of a $Cu/ZnO/Al_2O_3$ catalyst by XPS and TPD. Appl. Surf. Sci. 189:59-71.
[123] Raimondi F, Schnyder B, Kötz R, Schelldorfer R, Jung T, Wambach J, Wokaun A (2003) Structural changes of model Cu/ZnO catalysts during exposure to methanol reforming conditions. Surf. Sci. 532-535:383-389.
[124] Reitz TL, Lee PL, Czaplewski KF, Lang JC, Popp KE, Kung HH (2001) Time-resolved XANES investigation of CuO/ZnO in the oxidative methanol reforming reaction. J. Catal. 199:193-201.
[125] Knop-Gericke A, Hävecker M, Schedel-Niedrig T, Schlögl R (2001) Characterisation of active phases of a copper catalyst for methanol oxidation under reaction conditions: an in situ X-ray absorption spectroscopy study in the soft energy range. Top. Catal. 15:27-34.
[126] Klier K (1982) Methanol Synthesis. Adv. Catal. 31:243-313.
[127] Costantino U, Marmottini F, Sisani M, Montanari T, Ramis G, Busca G, Turco M, Bagnsco G (2005) Cu-Zn-Al hydrotalcites as precursors of catalysts for the production of hydrogen from methanol. Solid State Ionics 176:2917-2922.
[128] Larrubia Vargas MA, Busca G, Costantino U, Marmottini F, Montatnari T, Patrono P, Pinzari F, Ramis G (2007) An IR study of methanol steam reforming over ex-hydrotalcite Cu–Zn–Al catalysts. J. Mol. Catal. A 266:188-197.
[129] Busca G, Montanari T, Resini C, Ramis G, Costantino U (2009) Hydrogen from alcohols: IR and flow reactor studies. Catal. Today 143:2-8.
[130] Sakong S, Groß A (2003) Dissociative adsorption of hydrogen on strained Cu surfaces. Surf. Sci. 525:107-118.
[131] Girgsdies F, Ressler T, Wild U, Wübben T, Balk TJ, Dehm G, Zhou L, Günther S, Arzt E, Imbihl R, Schlögl R (2005) Strained thin copper films as model catalysts in the materials gap. Catal. Lett. 102:91-97.
[132] Hammer B, Nørskov JK (1995) Electronic factors determining the reactivity of metal surfaces. Surf. Sci. 343:211-220.
[133] Frost JC (1988) Junction Effect Interactions in Methanol Synthesis Catalysts. Nature 334:577-580.
[134] Zhang XR, Wang LC, Cao Y, Dai WL, He HY, Fan KN (2005) A unique microwave effect on the microstructural modification of $Cu/ZnO/Al_2O_3$ catalysts for steam reforming of methanol. Chem. Commun. 4104-4106.
[135] Wang LC, Liu YM, Chen M, Cao Y, He HY, Wu GS, Dai WL, Fan KN (2007) Production of hydrogen by steam reforming of methanol over Cu/ZnO catalysts prepared via a practical soft reactive grinding route based on dry oxalate-precursor synthesis. J. Catal. 246:193-204.
[136] Holladay JD, Wang Y, Jones E (2004) Review of Developments in Portable Hydrogen Production Using Microreactor Technology. Chem. Rev. 104:4767-4790.
[137] Kovnir K, Armbrüster M, Teschner D, Venkov TV, Jentoft FC, Knop-Gericke A, Grin Yu, Schlögl R (2007) A New Approach to Well-Defined, Stable and Site-Isolated Catalysts. Sci. Technol. Adv. Mater. 8:420-427.
[138] Kohlmann H (2002) Metal Hydrides. In: Encyclopedia of Physical Science and Technology, 3rd edn., Vol. 9, Academic Press, New York, 441-458.

[139] Friedrich M, Ormeci A, Grin Yu, Armbrüster M (2010) PdZn or ZnPd: Charge Transfer and Pd–Pd Bonding as the Driving Force for the Tetragonal Distortion of the Cubic Crystal Structure, Z. Anorg. Allg. Chem. 636:1735-1739.
[140] Armbrüster M, Schnelle W, Schwarz U, Grin Yu (2007) Chemical Bonding in $TiSb_2$ and VSb_2: A Quantum Chemical and Experimental Study. Inorg. Chem. 46:6319-6328.
[141] Armbrüster M, Schnelle W, Cardoso-Gil R, Grin Yu (2010) Chemical Bonding in the Isostructural Compounds $MnSn_2$, $FeSn_2$ and $CoSn_2$. Chem. European J. 16:10357-10365.
[142] Grin Yu, Wagner FR, Armbrüster M, Kohout M, Leithe-Jasper A, Schwarz U, Wedig U, von Schnering HG (2006) $CuAl_2$ Revisisted: Composition, Crystal Structure, Chemical Bonding, Compressibility and Raman Spectroscopy. J. Sol. State Chem. 179:1707-1719.
[143] Macchioni C, Rayne JA, Sen S, Bauer CL (1981) Low Temperature Resistivity of Thin Film and Bulk Samples of CuAl2 and Cu9Al4. Thin Solid Films 81:71-78.
[144] Iwasa N, Masuda S, Ogawa N, Takezawa N (1995) Steam Reforming of Methanol over Pd/ZnO: Effects of the Formation of PdZn Alloys Upon the Reaction. Appl. Catal. A 125:145-157.
[145] Miyao K, Onodera H, Takezawa N (1994) Highly Active Copper Catalysts for Steam Reforming of Methanol. Catalysts Derived from Cu/Zn/Al Alloys. React. Kinet. Catal. Lett. 53:379-383.
[146] Kameoka S, Tanabe T, Tsai AP (2004) Al-Cu-Fe Quasicrystals for Steam Reforming of Methanol: A New Form of Copper Catalyst. Catal. Today 93-95:23-26.
[147] Tanabe T, Kameoka S, Tsai AP (2006) A Novel Catalyst Fabricated from Al-Cu-Fe Quasicrystal for Steam Reforming of Methanol. Catal. Today 111:153-157.
[148] Yoshimura M, Tsai AP (2002) Quasicrystal Application on Catalyst. J. All. Compds. 342:451-454.
[149] Wallace WE, Elattar A, Imamura H, Craig RS, Moldovan, AG (1980) Intermetallic Compounds: Surface Chemistry, Hydrogen Absorption and Heterogeneous Catalysis. In: Wallace WE, Rao ECS (eds) Science and Technology of Rare Earth Materials, Academic Press, New York, 329-351.
[150] Nix RM, Rayment T, Lambert RM, Jennings JR, Owen G (1987) An *in situ* X-Ray Diffraction Study of the Activation and Performance of Methanol Synthesis Catalysts Derived from Rare-Earth-Copper Alloys. J. Catal. 106:216-234.
[151] Takahashi T, Kawabata M, Kai T, Kimura H, Inoue A (2006) Preparation of Highly Active Methanol Steam Reforming Catalysts from Glassy Cu-Zr Alloys with Small Amount of Noble Metals. Mater. Trans. 47:2081-2085.
[152] Bernal S, Calvino JJ, Cauqui MA, Gatica JM, Cartes CL, Omil JAP, Pintado JM (2003) Some Contributions of Electron Microscopy to the Characterisation of the Strong Metal-Support Interaction Effect. Catal. Today 77:385-406.
[153] Tauster SJ, Fung SC, Garten RL (1978) Strong Metal-Support Interactions. Group 8 Noble Metals Supported on TiO_2. J. Am. Chem. Soc. 100:170-175.
[154] Knözinger H, Taglauer E (2008) Spreading and Wetting. In: Ertl G, Knözinger H, Schüth F, Weitkamp J (eds) Handbook of Heterogeneous Catalysis, 2nd edn. Wiley-VCH, Weinheim, 555-571.
[155] Simoens AJ, Baker RTK, Dwyer DJ, Lund CRF, Madon RJ (1984) A Study of the Nickel-Titanium Oxide Interaction. J. Catal. 86:359-372.
[156] Centi G (2003) Metal-Support Interactions. In: Cornils B, Herrmann WA, Schlögl R, Wong CH (eds) Catalysis from A to Z, 2nd edn. Wiley-VCH, Weinheim, 490-491.
[157] Tauster SJ (1987) Strong Metal-Support Interactions. Acc. Chem. Res. 20:389-394.
[158] Penner S, Wang, D, Su DS, Rupprechter G, Podloucky, R, Schlögl R, Hayek K(2003) Platinum nanocrystals supported by silica, ceria and alumina: metal-support interactions due to high-temperature reduction in hydrogen. Surf. Sci. 532-535: 276.
[159] Penner S, Wang D, Podloucky R, Schlögl R, Hayek K (2004) Rh and Pt nanoparticles supported by CeO2: metal-support interaction upon high-temperature reduction observed by electron microscopy. Phys. Chem. Chem. Phys. 6: 5244.

[160] Iwasa N, Kudo S, Takahashi H, Masuda S, Takezawa N (1993) Highly Selective Supported Pd Catalysts for Steam Reforming of Methanol. Catal. Lett. 19:211-216.
[161] Takezawa N, Iwasa N (1997) Steam Reforming and Dehydrogenation of Methanol: Difference in the Catalytic Functions of Copper and Group VIII Metals. Catal. Today 36:45-56.
[162] Wang Y, Zhang J, Xu H (2006) Interaction Between Pd and ZnO during Reduction of Pd/ZnO Catalyst for Steam Reforming of Methanol to Hydrogen. Chin. J. Catal. 27:217-222.
[163] Wang Y, Zhang J, Xu H, Bai X (2007) Reduction of Pd/ZnO Catalyst and Its Catalytic Activity for Steam Reforming of Methanol. Chin. J. Catal. 28:234-238.
[164] Penner S, Jenewein B, Gabasch H, Klötzer B, Wang D, Knop-Gericke A, Schlögl R, Hayek K (2006) Growth and Structural Stability of Well-Ordered PdZn Alloy Nanoparticles. J. Catal. 241:14-19.
[165] Clark JB, Hastie JW, Kihlborg LHE, Metselaar R, Thackeray MM (1994) Definitions of Terms Relating to Phase Transitions of the Solid State. Pure & App. Chem. 66:577-594.
[166] Dagle RA, Chin YH, Wang Y (2007) The Effects of PdZn Crystallite Size on Methanol Steam Reforming. Top. Catal. 46:358-362.
[167] Karim A, Conant T, Datye A. (2006) The Role of PdZn Alloy Formation and Particle Size on the Selectivity for Steam Reforming of Methanol. J. Catal. 243:420-427.
[168] Lebarbier V, Dagle R, Datye A, Wang Y (2010) The Effect of PdZn Particle Size on Reverse-Water-Gas-Shift Reaction. Appl. Catal. A 379:3-6.
[169] Bollmann L, Ratts JL, Joshi AM, Williams WD, Pazmino J, Joshi YV, Miller JT, Kropf AJ, Delgass WN, Ribeiro FH (2008) Effect of Zn Addition on the Water-Gas Shift Reaction over Supported Palladium Catalysts. J. Catal. 257:43-54.
[170] Suwa Y, Ito SI, Kameoka S, Tomishige K, Kunimori K (2004) Comparative Study Between Zn-Pd/C and Pd/ZnO Catalysts for Steam Reforming of Methanol. Appl. Catal. A 267:9-16.
[171] Liu S, Takahashi K, Eguchi H, Uematsu K (2007) Hydrogen Production by Oxidative Methanol Reforming on Pd/ZnO: Catalyst Preparation and Supporting Materials. Catal. Today 129:287-292.
[172] Liu S, Takahashi K, Uematsu K, Ayabe M (2005) Hydrogen Production by Oxidative Methanol Reforming on Pd/ZnO. Appl. Catal. A 283:125-135.
[173] Liu S, Takahashi K, Ayabe M (2003) Hydrogen Production by Oxidative Methanol Reforming on Pd/ZnO Catalyst: Effect of Pd Loading. Catal. Today 87:247-253.
[174] Liu S, Takajashi K, Fuchigami K, Uematsu K (2006) Hydrogen Production by Oxidative Methanol Reforming on Pd/ZnO: Catalyst Deactivation. Appl. Catal. A 299:58-65.
[175] Liu S, Takahashi K, Uematsu K, Ayabe M (2004) Hydrogen Production by Oxidative Methanol Reforming on Pd/ZnO Catalyst: Effects of the Addition of a Third Metal Component. Appl. Catal. A 277:265-270.
[176] Lenarda M, Storaro L, Frattini R, Casagrande M, Marchiori M, Capannelli G, Uliana C, Ferrari F, Ganzerla R (2007) Oxidative Methanol Steam Reforming (OSRM) on a PdZnAl Hydrotalcite Derived Catalyst. Catal. Commun. 8:467-470.
[177] Cubeiro ML, Fierro JLG (1998) Partial Oxidation of Methanol Over Supported Palladium Catalysts. Appl. Catal. A 168:307-322.
[178] Cubeiro ML, Fierro JLG (1998) Selective Production of Hydrogen by Partial Oxidation of Methanol over ZnO-Supported Palladium Catalysts. J. Catal. 179:150-162.
[179] Agrell J, Germani G, Järås SG, Boutonnet M (2003) Production of Hydrogen by Partial Oxidation of Methanol Over ZnO-Supported Palladium Catalysts Prepared by Microemulsion Technique. Appl. Catal. A 242:233-245.
[180] Eastman JA, Thompson LJ, Kestel BJ (1993) Narrowing the Palladium-Hydrogen Miscibility Gap in Nanocrystalline Palladium. Phys. Rev. B 48:84-92.
[181] Yamauchi M, Ikeda R, Kitagawa H, Takata M (2008) Nanosize Effects on Hydrogen Storage in Palladium. J. Phys. Chem. C 112:3294-3299.

[182] Tew MW, Miller JT, van Bokhoven JA (2009) Particle Size Effect of Hydride Formation and Surface Hydrogen Adsorption of Nanosized Palladium Catalysts: L3 Edge vs K Edge X-Ray Absorption Spectroscopy. J. Phys. Chem. C 113:15140-15147.
[183] Ito SI, Suwa Y, Kondo S, Kamoeka S, Timishige T, Kunimori K (2003) Steam Reforming of Methanol over Pt-Zn Alloy Catalyst Supported on Carbon Black. Catal. Commun. 4:499-503.
[184] Iwasa N, Takezawa N (2003) New Supported Pd and Pt Alloy Catalysts for Steam Reforming and Dehydrogenation of Methanol. Top. Catal. 22:215-224.
[185] Lim KH, Chen ZX, Neyman KM, Rösch N (2006) Comparative Theoretical Study of Formaldehyde Decomposition on PdZn, Cu, and Pd Surfaces. J. Phys. Chem. B 110:14890-14897.
[186] Lorenz H, Zhao Q, Turner S, Lebedev BL, Van Tendeloo G, Klötzer B, Rameshan C, Pfaller K, Konzett J, Penner S (2010) Origin of Different Deactivation of Pd/SnO_2 and Pd/GeO_2 Catalysts in Methanol Dehydrogenation and Reforming: A Comparative Study. Appl. Catal. A 381:242-252.
[187] Penner S, Lorenz H, Jochum W, Stöger-Pollach M, Wang D, Rameshan C, Klötzer B (2009) Pd/Ga_2O_3 Methanol Steam Reforming Catalysts: Part I. Morphology, Composition and Structural Aspects. Appl. Catal. A 358:193-202.
[188] Kovnir K, Schmidt M, Waurisch C, Armbrüster M, Prots Yu, Grin Yu (2008) Refinement of the Crystal Structure of Dipalladium Gallide, Pd_2Ga. Z. Kristallogr. - New Crystal Structures 223:7-8.
[189] Lorenz H, Turner S, Lebedev OI, Van Tendeloo G, Klötzer B, Rameshan C, Pfaller K, Penner S (2010) $Pd–In_2O_3$ Interaction Due to Reduction in Hydrogen: Consequences for Methanol Steam Reforming. Appl. Catal. A 374:180-188.
[190] Kamiuchi N, Muroyama H, Matsui T, Kikuchi R, Eguchi K (2010) Nano-Structural Changes of SnO_2-Supported Palladium Catalysts by Redox Treatments. Appl. Catal. A 379:148-154.
[191] Teschner D, Borsodi J, Wootsch A, Révay Z, Hävecker M, Knop-Gericke A, Jackson SD, Schlögl R (2008) The Roles of Subsurface Carbon and Hydrogen in Palladium-Catalyzed Alkyne Hydrogenation. Science 320:86-89.
[192] Teschner D, Révay Z, Borsodi J, Hävecker M, Knop-Gericke A, Schlögl R, Milroy D, Jackson SD, Torres D, Sautet P (2008) Understanding Palladium Hydrogenation Catalysts: When the Nature of the Reactive Molecule Conrols the Nature of the Catalyst Active Phase. Angew. Chem. Int. Ed. 47:9274-9278.
[193] Seriani N, Mittendorfer F, Kresse G (2010) Carbon in Palladium Catalysts: A metastable Carbide. J. Chem. Phys. 132: 024711.
[194] Al Alam AF, Matar SF, Nakhl M, Quaini N (2009) Investigations of Changes in Crystal and Electronic Structures by Hydrogen within $LaNi_5$ from First-Principles. Sol. State Sci. 11:1098-1106.
[195] Kohout M (2004) A Measure of Electron Localizability. Int. J. Quant. Chem. 97:651-658.
[196] Kohout M, Wagner FR, Grin Yu (2006) Atomic Shells from the Electron Localizability in Momentum Space. Int. J. Quant. Chem. 106:1499-1507.
[197] Kohout M (2007) Bonding Indicators from Electron Pair Density Functionals. Faraday Disc. 135:43-54.
[198] Kovnir K, Armbrüster M, Teschner D, Venkov TV, Szentmiklósi L, Jentoft FC, Knop-Gericke A, Grin Yu, Schlögl R (2009) *In situ* Surface Characterization of the Intermetallic Compound PdGa – A Highly Selective Hydrogenation Catalyst. Surf. Sci. 603:1784-1792.
[199] Osswald J, Giedigkeit R, Jentoft RE, Armbrüster M, Girgsdies F, Kovnir K, Grin Yu, Ressler T, Schlögl R (2008) Palladium Gallium Intermetallic Compounds for the Selective Hydrogenation of Acetylene. Part I: Preparation and Structural Investigation Under Reaction Conditions. J. Catal. 258:210-218.
[200] Osswald J, Kovnir K, Armbrüster M, Giedigkeit R, Jentoft RE, Wild U, Grin Yu, Schlögl R (2008) Palladium Gallium Intermetallic Compounds for the Selective Hydrogenation of

Acetylene. Part II: Surface Characterization and Catalytic Performance. J. Catal. 258:219-227.
[201] Chen ZX, Neyman KM, Gordienko AB, Rösch N (2003) Surface Structure and Stability of PdZn and PtZn Alloys: Density Functional Slab Model Studies. Phys. Rev. B 68:075417.
[202] Bayer A, Flechtner K, Denecke R, Steinrück HP, Neyman KM, Rösch N (2006) Electronic Properties of Thin Zn Layers on Pd(111) During Growth and Alloying. Surf. Sci. 600:78-94.
[203] Chen ZX, Neyman KM, Rösch N (2004) Theoretical Study of Segregation of Zn and Pd in Pd-Zn Alloys. Surf. Sci. 548:291-300.
[204] Chen ZX, Neyman KM, Gordienko AB, Rösch N (2003) Surface Structure and Stability of PdZn and PtZn Alloys: Density-Functional Slab Model Studies. Phys. Rev. B 68:075417.
[205] Chen ZX, Neyman KM, Lim KH, Rösch N (2004) CH_3O Decomposition on PdZn(111), Pd(111), and Cu(111). A Theoretical Study. Langmuir 20:8068-8077.
[206] Chen ZX, Lim KH, Neyman, KM, Rösch N (2004) Density Functional Study of Methoxide Decomposition on PdZn(100). Phys. Chem. Chem. Phys. 6:4499-4504.
[207] Chen ZX, Lim KH, Neyman KM, Rösch N (2005) Effect of Steps on the Decomposition of CH_3O at PdZn Alloy Surfaces. J. Phys. Chem. B 109:4568-4574.
[208] Fasana A, Abbati I, Braicovich L (1982) Photoemission Evidence of Surface Segregation at Liquid-Nitrogen Temperature in Zn-Pd System. Phys. Rev. B 26:4749-4751.
[209] Rodriguez JA (1994) Interactions in Bimetallic Bonding: Electronic and Chemical Properties of PdZn Surfaces. J. Phys. Chem. 98:5758-5764.
[210] Stadlmayr W, Penner S, Klötzer B, Memmel N (2009) Growth, Thermal Stability and Structure of Ultrathin Zn-Layers on Pd(111). Surf. Sci. 603:251-255.
[211] Rameshan C, Stadlmayr W, Weilach C, Penner S, Lorenz H, Hävecker M, Blume R, Rocha T, Teschner D, Knop-Gericke A, Schlögl R, Memmel N, Zemlyanov D, Rupprechter G, Klötzer B (2010) Subsurface-Controlled CO_2 Selectivity of PdZn Near-Surface Alloys in H_2 Generation by Methanol Steam Reforming. Angew. Chem. Int. Ed. 49:3224-3227.
[212] Stadlmayr W, Rameshan C, Weilach C, Lorenz H, Hävecker M, Blume R, Rocha T, Teschner D, Knop-Gericke A, Zemlyanov D, Penner S, Schlögl R, Rupprechter G, Klötzer B, Memmel N (2010) Temperature-Induced Modifications of PdZn Layers on Pd(111). J. Phys. Chem. C 114:10850-10856.
[213] Weirum G, Kratzer M, Koch HP, Tamtögl A, Killmann J, Bako I, Winkler A, Surnev S, Netzer FP, Schennach R (2009) Growth and Desorption Kinetics of Ultrathin Zn Layers on Pd(111). J. Phys. Chem. C 113:9788-9796.
[214] Koch HP, Bako I, Weirum G, Kratzer M, Schennach R (2010) A Theoretical Study of Zn Adsorption and Desorption on a Pd(111) Substrate. Surf. Sci. 604:926-931.
[215] Gabasch H, Knop-Gericke A, Schlögl R, Penner S, Jenewein B, Hayek K, Klötzer B (2006) Zn Adsorption on Pd(111): ZnO and PdZn Alloy Formation. J. Phys. Chem. B 110:11391-11398.
[216] Jeroro E, Vohs JM (2008) Zn Modification of the reactivity of Pd(111) Toward Methanol and Formaldehyde. J. Am. Chem. Soc. 130:10199-10207.
[217] Jeroro E, Lebarbier V, Datye A, Wang Y, Vohs JM (2007) Interaction of CO with Surface PdZn Alloys. Surf. Sci. 601:5546-5554.
[218] Massalski TB (1990) Pd-Zn (Palladium-Zinc). In: Masaalski TB (ed) Binary Alloy Phase Diagrams, 2nd edn. ASM International, Materials Park, 3068-3070.
[219] Iwasa N, Mayanagi T, Masuda S, Takezawa N (2000) Steam Reforming of Methanol over Pd-Zn Catalysts. React. Kinet. Catal. Lett. 69:355-360.